OSTI Topical Report

FUSION RESEARCH CENTER

DOE/ER/542-41-163 FRCR #484

Compact Tokamak Reactors
Part 1 (analytic results)

A. J. Wootton, J. C. Wiley, P. H. Edmonds, D. W. Ross

Fusion Research Center
The University of Texas at Austin
Austin, TX 78712

September 1996

THE UNIVERSITY OF TEXAS

Austin, Texas

September 13, 1996

Compact Tokamak Reactors
Part 1 (analytic results)

A. J. Wootton, J. C. Wiley, P. H. Edmonds and D. W. Ross

Fusion Research Center,

University of Texas at Austin,

Austin, TX 78712, USA

We discuss the possible use of tokamaks for thermonuclear power plants, in particular tokamaks with low aspect ratio and copper toroidal field coils. Three approaches are presented. First we review and summarize the existing literature. Second, using simple analytic estimates, the size of the smallest tokamak to produce an ignited plasma is derived. This steady state energy balance analysis is then extended to determine the smallest tokamak power plant, by including the power required to drive the toroidal field, and considering two extremes of plasma current drive efficiency. The analytic results will be augmented by a numerical calculation which permits arbitrary plasma current drive efficiency; the results of which will be presented in Part II. Third, a scaling from any given reference reactor design to a copper toroidal field coil device is discussed. Throughout the paper the importance of various restrictions is emphasized, in particular plasma current drive efficiency, plasma confinement, plasma safety factor, plasma elongation, plasma beta, neutron wall loading, blanket availability and recirculating electric power. We conclude that the latest published reactor studies, which show little advantage in using low aspect ratio unless remarkably high efficiency plasma current drive and low safety factor are combined, can be reproduced with the analytic model.

Contents

1. Introduction

The purpose of this document is to present a simple steady state model, complementing published numerical results, on possible tokamak power plants. Emphasis is placed on the possible utility of low-aspect-ratio devices, with normal copper toroidal field coils. Low-aspect-ratio (LAR) tokamaks have been proposed as possible neutron sources and as maintainable fusion power plants with a competitive cost of electricity [1]. Here the aspect ratio $A = R/a$ with R the major radius and a the minor radius of the plasma. One of their possible advantages is compactness; a smaller device (either size or power output, or both) might be built at low aspect ratio $A \leq 2$ than at normal aspect ratio $A \approx 3.5$.

In order to achieve the lowest aspect ratios the minimum of material must be used at the inner equator. This either precludes the use of a neutron shield, or at best permits only a thin shield, in this location. Superconducting coils cannot be used in the environment of the fusion generated neutron flux; no poloidal field coils and a normal copper toroidal field coil inner leg are implied. This copper toroidal field coil inner leg must be considered sacrificial; with a neutron flux equivalent to ≈ 5 MWm^{-2} replacement would be necessary every few months [2].

The literature survey presented below summarizes the results of different groups using various predictive models to determine the parameters of possible tokamak power plants [3 to 12]. In many cases it is not obvious why a given solution has been found, and in comparisons between different predictions it is not always clear what parameters have been held constant. In particular, the literature survey shows emphasis on superconducting coil devices with $A \approx 4$ and normal copper coil devises with $A \approx 1.3$; normal copper coil devices with $A > 1.3$ are not generally considered.

The analytic model presented here uses an assumed scaling relationship for the plasma energy confinement time, together with various constraints, to deduce an expression for the geometry of possible ignited tokamaks and power plants. We do not address the cost of electricity (CoE), which is considered outside the scope of a simple analytic model. Rather the device with the smallest major radius, and thus the smallest volume, is found as A is varied. There is an assumed relationship between smaller machine encompassing volume (the size of the box into which the plasma would fit) and increased attractiveness. The

results, intended to complement the more sophisticated numerical studies, allow comparisons between machines of arbitrary A. The particular scaling relation used is due to Goldston [13,14], and is chosen because of the simplicity of the resulting analysis. Allowance for various confinement regimes is introduced by a confinement improvement factor H. Extensions to other scaling relations will be discussed in Part II. Our present state of knowledge of plasma confinement precludes a better analysis; equivalent assumptions are used in the already-published studies.

The steady-state energy balance equation ignores radiation losses, which are therefore assumed either small or to be described by a global energy confinement time. With the assumed scaling for the energy confinement time, the major radius R of the tokamak is related to the plasma current I_p, which in turn is related to the safety factor q and the toroidal field B_T. The smallest device is then obtained by operating at the lowest q and highest B_T. If B_T is produced by superconducting coils, then the maximum possible value in the plasma is restricted by the maximum permitted at the coil surface. If copper toroidal field coils are used, then the maximum value in the plasma is restricted by the power required to produce the field.

Two considerations impose restrictions on the minimum possible q. First, at normal $A \approx 3.5$, experimental observation supported by stability theory requires $q \gtrsim 3$. There is both experimental and theoretical evidence that higher values of q are required as A is reduced [12,15,16]. If the power required to drive the plasma current was zero (i.e. completely efficient auxiliary current drive), this restriction would give the smallest machine. High efficiency current drive might result from using the direct reflection of cyclotron radiation [17]. The case of totally inefficient auxiliary current drive can also be considered. In this case the plasma current must be driven by a bootstrap mechanism; requiring 100% bootstrap current ($f_{bs} = 1$) generally imposes a higher limit on q than does stability. Throughout the paper we use 'bootstrap current' to mean bootstrap plus diamagnetic plus Pfirsch-Schluter currents [18], that is, the part of the plasma current which need not be produced by auxiliary current drive techniques. Requiring $f_{bs} = 1$ completely prescribes the pressure and plasma current density profiles, rendering the analysis presented inconsistent and the machine uncontrollable. Under these circumstances auxiliary plasma current drive would still be needed, to tailor the total plasma current profile to that required. Partly for this reason the numerical modeling was developed, which allows arbitrary current drive efficiencies. Nevertheless the $f_{bs} = 1$ limit is instructive, allowing analytic comparisons to be made between devices with different A. In particular

it allows a comparison (within the model restrictions) of the size and parameters of the smallest possible reactor, and of the size necessary to produce a given electric power to the grid (up to a known limit), e.g. P_{gr} = 1 GW, as a function of A.

The constraints on B_T and q are cast in terms of a permitted recirculating power fraction χ, and must incorporate certain restrictions. The most important of these is the permissible neutron-power wall loading. Generally it is this, together with the confinement time (the H factor), which determines the machine size. Second is the maximum toroidal beta (the ratio of plasma pressure to magnetic field pressure) which can be tolerated. For simplicity we use β_T, the ratio of volume averaged plasma pressure to the toroidal field pressure in vacuum on axis. This can also be cast in terms of a theoretical scaling, the Troyon scaling, which explains existing experimental data [19]. The multiplier acting on the scaling relationship value is called the normalized beta, or β_N. Arbitrarily increasing the H factor is not useful unless the maximum β_T permitted is also increased. Lastly is the restriction that the plasma density n does not exceed the experimentally deduced empirical upper limit, the Greenwald density limit [20], while the plasma temperature T remains within the validity of the approximations used.

Finally, we note that the analysis presented considers only the efficacy of the final ignited state. That is, we do not discuss the feasibility or practicality of attaining this state - is there any route, let alone a cost effective route, to ignition?. Also, the stability of the final ignited state is not discussed.

2. A Survey of Low Aspect Ratio Reactor Designs

A survey of various reactor designs has been completed, concentrating on results since 1990 [2 to 12]. A number of low-A studies were identified which included an estimate of the cost of electricity (CoE). Comparable studies for standard aspect ratio (normal-A) designs and for a spheromak reactor [8] are included. The most complete studies are those by the ARIES group, using the Aries System Code (ASC) and by Perkins and Galambos et al., using SuperCode. Table 1 is a summary of the basic parameters associated with each design. Many of the designs described are extracted from ongoing programs and so represent a snapshot in time of the project progress; later iterations may improve the predicted performance.

A number of points are to be noticed. We consider first the normal-A superconducting designs, concentrating on the Aries/Starlite studies. With the passage of time the machine size has in general been reduced, primarily by including advanced tokamak scenarios (i.e. increased confinement, high β_T, high f_{bs}) with a corresponding reduction in the cost of electricity (CoE). The most attractive design is the Reversed Shear configuration; this also has the most physics uncertainty associated with the need to maintain the reverse shear profiles and high bootstrap fraction through some mix of external current drive scenarios. Second we consider the low-A designs. The Aries/Starlite low-A LAR designs can be most accurately compared with the normal-A results; however the LAR designs are for a copper toroidal field magnet with a 0.3 m shield while the standard designs are superconducting. Overall the trend, with the passage of time and improved reality in the models, is for an increase in predicted size and CoE. This trend is mainly due to the more proper inclusion of the cost of the recirculating power associated with the resistive toroidal field center post and the current drive requirements (a feature of low-A designs is the extremely large plasma current). The most recent design LAR-2 has essentially 100% bootstrap current.

Table I. Parameter Summary for Selected Reactor Studies

Study	Yr	A	R m	κ	I_p MA	f_{bs} %	H (a)	β_N	β_T %	Γ_n (e)	χ %	CoE (b)	P_{gr} GW
SS[3]	95	4.0	5.8	1.8	7	87	2.9	5.3	3.0	4.9[f]	17	78[c]	1.0
RS[3]	95	4.5	5.5	1.8	10	84	2.1	4.1	4.0	5.4[f]	14	81[c]	1.0
FS[3]	95	4.0	7.8	1.6	13	57	1.7	2.9	2.0	2.7[f]	29	102[c]	1.0
PU[3]	95	4.0	7.9	1.6	15	34	2.4	2.7	2.5	2.2[f]	6	123[c]	1.0
Aries-IA[4]	94	4.0	7.4		11	65	1.8	3.2	2.3	2.1	28	108	1.0
SSCD[5] β_N=4	94	2.87	6	2	21	37	1.9	4.0	7.2	2.6		130	1.0
SSCD[5] β_N=6	94	3.21	5.1	2	13	62	2.6	6.0	9.3	3.5		103	1.0
EEF-R2[11]	92	3.8	5.3	2.3	17				7.6	4.2	20		1.2
Aries-I[4]	90	4.5	6.7		11	65	1.8	3.2	1.9	3	28	65	1.0
LAR-2[6]	96	1.25	5.0	3.4	40	100	3.0	6.4	36	2.2	63	116	1.0
GA-Demo[7]	96	1.4	2.1		25	90	3.5		62				1.3
LAR-1[3]	95	1.25	5.6	2.2	39	85	2.4	7.9	39	3.9[f]	63	132	1.0
CSR[8]	94	1.25	1.67		48				10		16	60	1.0
TARTR[9]	92	1.4	1.42	2.3	29	70	2.6[d]						0.8
STR[10]	92	1.3	1.4	2.7	22	75			>50	18			0.5
TARR-a[11,12]	92	1.3	2.26	2.3	35	65	0.8	3.5		10	33	85	1.2
TARR-b[11,2]	92	1.3	1.97	2.3	30	66	1[d]	3.5		9.4	38	99	0.8
TARR-c[11,2]	92	1.3	1.79	2.3	25	67	1.5[d]	3.5		6.5	46	137	0.4
TARR-d[11,2]	92	1.3	1.87	2.3	25	62	1.2[d]	3.3		6.3	50	150	0.4
TARR-e[11,2]	92	1.3	1.96	2.3	28	58	1.3[d]	3.0		5.8	50	151	0.4
TARR-g[11,2]	92	1.3	1.61	2.3	23	100	1.8[d]	3.5		7.2	39	114	0.4

Notes: (a) ITER-89P scaling [21] unless stated otherwise.
(b) mill/kWeh, unless otherwise stated w/o safety credits (LSA = 4).
(c) Costed in 1992 $.
(d) H factor with respect to Rebut-Lallia scaling [22].
LSA Levels of Safety Assurance, for which credits are taken in the CoE where noted in the particular reference [23].
(e) average first wall neutron energy flux, MWm^{-2}, unless otherwise noted.
(f) peak first wall neutron energy flux, MWm^{-2}.
Other symbols are defined in subsequent sections.

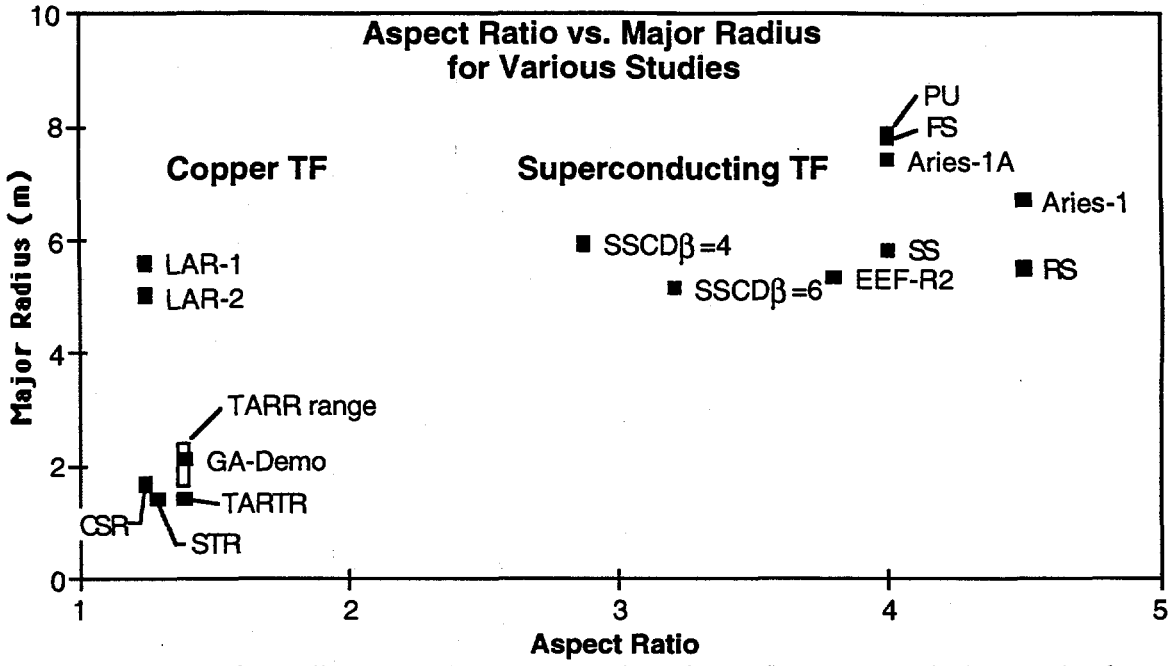

Figure 1. The major radius R_0 against aspect ratio A for various reactor designs. The data point labels are identified in Table 1 and in the list of references [2 to 12]. The open box is intended to cover the range of TARR parameters.

Figure 1, in which the major radius of the various designs considered is plotted as a function of aspect ratio, summarizes the studies discussed. It is concluded that the designs for normal-A ($A \approx 4$) and for the two most recent low-A devices (LAR-1 and LAR-2) with $A \approx 1.25$ now have essentially the same major radius R_0 for equivalent generated power. However the normal-A devices have a lower CoE. Both these trends reflect no advantage to low-A designs. Indeed, the machine encompassing volume

$$V_m = 2\pi\kappa R_0^3 \frac{(A+1)^2}{A^3} \tag{1}$$

where κ is the elongation, is larger for the most recent low-A designs than for the most recent normal-A designs. This is because, even at constant R_0 and κ, V_m increases as A decreases.

There is a grouping of low-A designs with $A \approx 1.25$ and $R_0 \approx 2$ m in which R_0 is significantly less than the value of both the most recent LAR-1 and LAR-2 designs, and less than all the normal-A superconducting designs. The most detailed information for devices within this low-A grouping exists for TARTR [9] and TARR [11,12]. These all operate at comparatively low safety factor ($q \approx 5$), and produce the required plasma current

by a mix of bootstrap current and highly efficient auxiliary current drive using reflected radiation [16]. This untested scheme relies on the small cyclotron power loses (≈ 1 MW) and asymmetric reflecting walls, to drive ≈ 10 MA of plasma current. The CSR is a spheromak design, with assumptions outside the scope of the analysis presented later.

To conclude this section, the literature survey shows that a low-A, steady-state, copper-magnet reactor would be larger (a larger V_m) and more expensive (larger CoE) than a normal-A superconducting magnet reactor. This result is driven by the requirement for large plasma current at low-A and the need to minimize recirculating power and hence for large bootstrap fractions. The exception is if a very efficient current drive scheme can be used, in conjunction with a low value of safety factor. These conclusions are supported by, and understandable from, the analysis presented in the following sections.

3. The Analytic Model

An equation relating the major radius of an ignited tokamak to the safety factor and toroidal field is derived. Constraints are then applied relevant to either normal copper toroidal field coils, or superconducting coils, and the geometry of the smallest device found. Although the analysis allows many parameters to be derived (e.g. power to the grid), we concentrate on those related directly to the geometry.

3.1. Power Flows

Here we present the analytic model of a steady state tokamak and tokamak power plant, which allows us to deduce the minimum device size. The emphasis is on devices with normal copper toroidal field coils, although superconducting coil devices are discussed. The power flows considered are shown in *Figure 2*. The externally supplied power to the plasma, P_{in}^{ext}, is the sum of the additional heating power P_H and the power required to drive the plasma current, P_{CD}. The power required to produce the toroidal field is P_{TF}. The alpha particle power, assumed all deposited in the plasma, is P_α. The neutron power P_n is converted to electric power P_{el} with an efficiency f_{el}. The electric power is converted to heating, current drive and toroidal field power with efficiencies f_H, f_{CD} and f_{TF}. The power to the grid is P_{gr} No benefit is taken for the heat generated in producing the toroidal field, or the heat incident on plasma facing components (= W/τ_E).

The plasma stored energy W is determined by the total heating power ($= P_H + P_{CD} + P_\alpha$) and an energy confinement time τ_E. That is, we assume that any auxiliary current drive power not only drives a plasma current, but also heats the plasma. We will also assume that both the heating and current drive power degrade the energy confinement time. While other losses (e.g. Bremsstrahlung, synchrotron radiation) would occur in practice, we assume for simplicity that they are covered by the confinement time scaling relationship.

3.2. Machine Architecture

Here the objective is to derive an expression for the major radius of an ignited deuterium-tritium fueled tokamak. We utilize the parameter $F = P_\alpha / (W/\tau_E)$; F is related to $Q_n = P_n / P_{in}^{ext}$ by $Q_n \approx 4F/(1-F)$, with the factor 4 appearing because $P_n \approx 4P_\alpha$. If there is no auxiliary current drive power then the condition for ignition is $Q_n = \infty$ or $F = 1$. With auxiliary current drive the condition is modified, as discussed later.

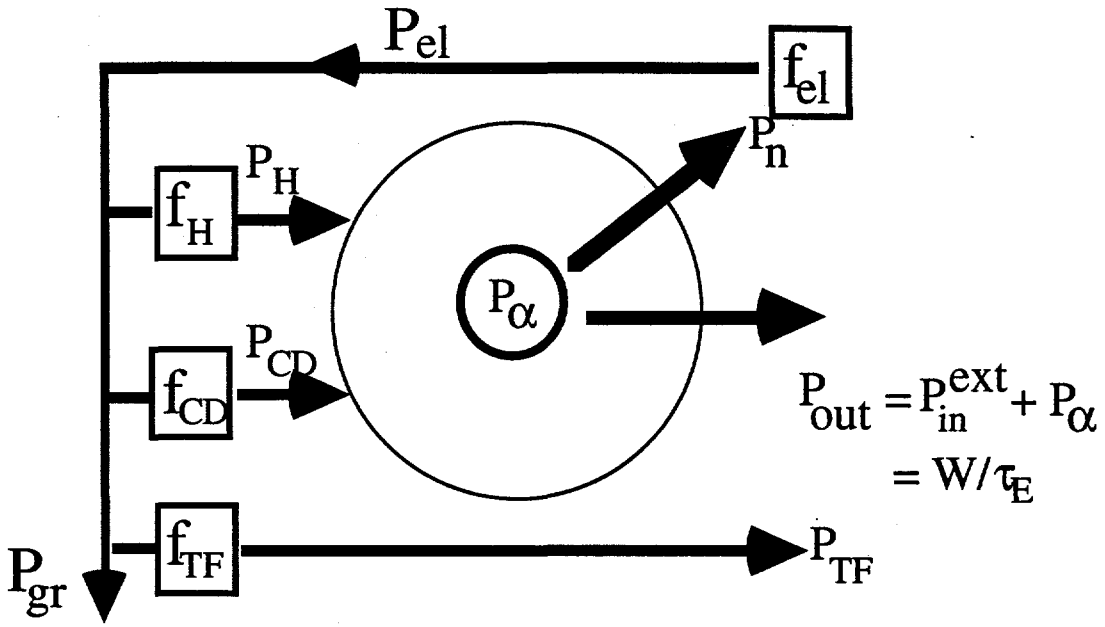

Figure 2. The power flows and efficiencies considered. f_{el} is the efficiency of conversion from neutron power (P_n) to electric power P_{el}. The efficiencies of conversion from electric power P_{el} to toroidal field power (P_{TF}), auxiliary current drive power (P_{CD}) and heating power (P_H) are f_{TF}, f_{CD} and f_H. The plasma is heated by P_H , the alpha particle power P_α, and P_{CD} to produce a stored energy W and energy confinement time τ_E.

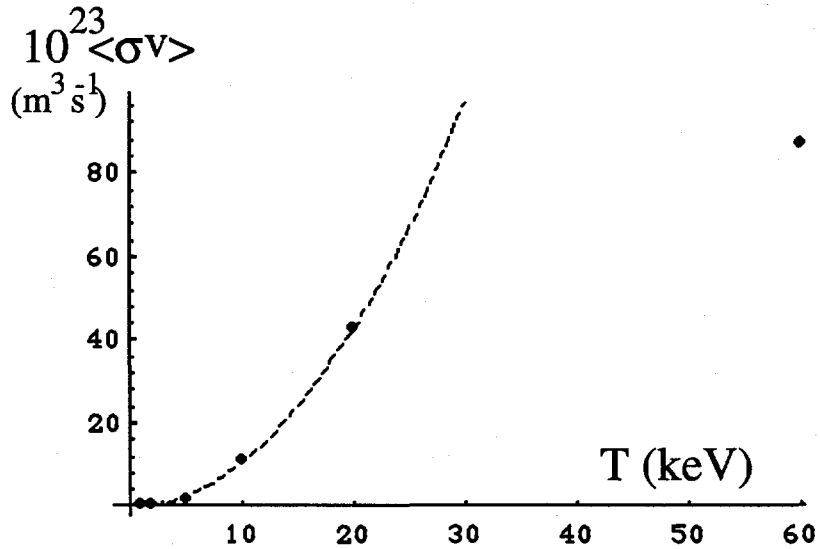

Figure 3. The (cross section times velocity) for D-T reactions, integrated over a Maxwellian distribution. The points are taken from a table given in Glasstone and Loveberg's 'Controlled Thermonuclear Reactions', the solid line is the fit $\langle \sigma v \rangle (m^3 s^{-1}) = 1.08 x 10^{-24} T^2 (keV)$.

For a D-T plasma the power associated with the alpha particles (the alpha power) produced is $P_\alpha = \int n_D n_T \langle \sigma v \rangle Q_{DT} dV$, where Q_{DT} = 3.5 MeV = 5.6x10^{-13} W. For a D-T Maxwellian plasma with the reacting temperature T between 5 and 20 keV, *Figure 3* shows that the D-T reaction rate $\langle \sigma v \rangle \propto T^2$. The alpha power P_α can then be written as (for equal deuterium and tritium densities, $n_D = n_T$)

$$P_\alpha(\mathrm{W}) = 1.5 \times 10^{-37} \langle nT \rangle^2 V \frac{g^2 (1+\gamma_n+\gamma_T)^2}{1+2(\gamma_n+\gamma_T)}, \tag{2}$$

where V is the plasma volume ($V = 2\pi^2 \kappa R_0 a^2$ for an elliptic cross-sectioned plasma; corrections for triangularity are found in Appendix 1), $\langle \ldots \rangle$ denotes a volume average, the profiles of density n(m^{-3}) and temperature T(keV) are given by the following functions of γ_n and γ_T:

$$n, T = n_0, T_0 \left[1 - (r/a)^2\right]^{\gamma_n, \gamma_T},$$

and

$$g \equiv \left(Z_i - Z_{eff}\right) / \left(Z_i - 1\right)$$

accounts for fuel dilution. Unless otherwise specified, n denotes electron density. Then,

$$F = 3.2 \times 10^{-22} \langle nT \rangle \tau_E \frac{g^2 (1+\gamma_n+\gamma_T)^2}{g_2 \left(1+2(\gamma_n+\gamma_T)\right)}, \tag{3}$$

where

$$g_2 \equiv \left(2Z_i + 1 - Z_{eff}\right) / \left(2Z_i\right)$$

accounts for pressure dilution. Using energy balance we obtain

$$F = \frac{2 \times 10^{-6} P_\Sigma \tau_E^2}{3V} \frac{g^2 (1+\gamma_n+\gamma_T)^2}{g_2^2 \left(1+2(\gamma_n+\gamma_T)\right)}, \tag{4}$$

where $P_\Sigma = P_\alpha + P_{CD} + P_H$ is the total heating power (external plus alpha).

To proceed further, an expression for $P_\Sigma \tau_E^2 / V$ in terms of A is required. Consider scaling relations for τ_E of the form proposed by Goldston [13,14];

$$\tau_E(\mathrm{s}) = c\, H\, I_p(\mathrm{A})^{\alpha_I} P_\Sigma(\mathrm{W})^{-0.5} \kappa^{0.5} R_0(\mathrm{m})^{\alpha_R} a(\mathrm{m})^{\alpha_a}, \tag{5}$$

where for L mode $c = 3.7\times10^{-5}\sqrt{2.5/1.5}$, with the factor in the square root accounting for the isotope effect for a D-T mixture, $\alpha_R = 1.75$, and $\alpha_a = -0.37$. The factor H describes any improvement in confinement over L mode. No explicit density or toroidal field (B_T) dependence is considered. The form of the scaling with power is important, because in this particular case F is independent of power. The parameters α_R and α_a are left free in order to investigate how their uncertainty affects the final results. Using Equations (4) and (5), we find that

$$F = \frac{2\times10^{-6} c^2 H^2 I_p{}^2 \kappa R_0^{2\alpha_R} a^{2\alpha_a}}{3V} \frac{g^2\left(1+\gamma_n+\gamma_T\right)^2}{g_2^2\left(1+2\left(\gamma_n+\gamma_T\right)\right)} \tag{6}$$

in MKS units. The objective is to observe how this parameter varies as A is reduced, with certain constraints applied. Equation (6) can be written approximately as $F \propto \left(I_p A\right)^2$; that is, reducing A degrades F, and the loss must be made up by using a larger I_p.

The plasma current I_p in Equation (6) is assumed to be restricted by the edge safety factor q, which is taken in the form of a fit to numerical and analytic low-A equilibria [24]:

$$q = q_{\rm cyl}\left(1.22-\frac{0.68}{A}\right)\left(1-\left(\frac{1}{A}\right)^2\right)^{-2}, \tag{7}$$

with the large aspect-ratio (cylindrical) part given by

$$q_{\rm cyl} = \frac{2\pi a^2 B_{T0}}{\mu_0 I_p R_0}\left(\frac{1+\kappa^2\left(1+2\delta^2-1.2\delta^3\right)}{2}\right). \tag{8}$$

(Throughout this document we use q rather than q_ψ to denote the true safety factor.)

The plasma surface is described by the equation $R = R_0 + x$ with $x = a\cos\left(\alpha+\delta\sin\alpha\right)$ and $y = a\kappa\sin\alpha$, where δ is the triangularity and κ the vertical elongation of the cross section (see Appendix 1). Note that q as written does not give the correct limit as $A\rightarrow\infty$, but is well suited to the values of A considered here. The toroidal field B_{T0} in Equation (8) is the vacuum field at the plasma geometric axis, which is given by

$$B_{T0} = B_{Tleg}\frac{(A-1)}{A}\left(1-\frac{w_b A}{R_0(A-1)}\right) \tag{9}$$

where w_b is the distance between the plasma inner equator and the TF coil (i.e. the shield, or blanket, thickness). That is, B_{T0} is related to the field B_{Tleg} at the inner toroidal-field-coil leg. For much of the work described we will assume no shield at the inner equator (giving advantage to low-A), so that

$$B_{T0} = B_{Tleg}\frac{(A-1)}{A} \tag{10}$$

The expression for the plasma volume (see Appendix 1), Equation (6) for F, Equations (7) and (8) for the plasma current in terms of the safety factor q, and Equation (9) for the toroidal field, can be combined to give the major radius required to produce a specified F at a given aspect ratio,

$$R_0\left(1-\frac{w_b A}{R_0(A-1)}\right)^{\frac{2}{(2\alpha_R-1+2\alpha_p)}} = \left(\frac{Fq^2 f_2(\delta,A)}{\lambda B_{Tleg}^2 f_1(A) f_3(\delta,\kappa)}\right)^{\frac{1}{(2\alpha_R-1+2\alpha_p)}} \tag{11}$$

where

$$\lambda = \frac{10^8 c^2 H^2 g^2 (1+\gamma_n+\gamma_T)^2}{48\pi^2 g_2^2 (1+2(\gamma_n+\gamma_T))} \tag{12}$$

and the functions $f_1(A)$, $f_2(\delta,A)$ and $f_3(\delta,\kappa)$ are

$$f_1(A) = \left(\frac{\left(1.22-\frac{0.68}{A}\right)^2 (A-1)^2}{\left(1-\left(\frac{1}{A}\right)^2\right)^4 A^{4+2\alpha_a}}\right) \tag{13}$$

$$f_2(\delta,A) = \left(1-\frac{\delta}{4A}-\frac{\delta^2}{8}\right) \tag{13a}$$

$$f_3(\delta,\kappa) = \left(1+\kappa^2\left(1+2\delta^2-1.2\delta^3\right)\right)^2 \tag{14}$$

Because $\left(2\alpha_R-1+2\alpha_p\right) = 1.76 \approx 2$ we can approximate the solution of Equation (11) by

$$R_0 = \left(\frac{Fq^2 f_2(\delta,A)}{\lambda B_{Tleg}^2 f_1(A) f_3(\delta,\kappa)}\right)^{\frac{1}{(2\alpha_R-1+2\alpha_p)}} + \frac{w_b A}{(A-1)}. \tag{15}$$

In the case of no inner shield (toroidal field given by Equation (10)), then the exact solution is

$$R_0 = \left(\frac{Fq^2 f_2(\delta, A)}{\lambda B_{Tleg}^2 f_1(A) f_3(\delta, \kappa)} \right)^{\frac{1}{(2\alpha_R - 1 + 2\alpha_p)}} \tag{16}$$

The major radius R_0 is a function of aspect ratio A, confinement characteristics (c, H, α_R, α_a), the profiles (γ_T, γ_n), the impurity dilution (g, g_2), the shaping factors (κ, δ), the operational value of safety factor q and the toroidal field at the TF leg surface B_{Tleg}. The parameters F, q and B_{Tleg} must now be chosen. Finding below that $F = 1$ for ignition (when $P_{CD} = 0$) then we seek relationships between R_0, q and B_{Tleg}.

3.3. Constraints

3.3.1. Normal Copper TF Coils

In this case we are working with Equation (16) (i.e. no inner shield, advantaging low-A). To choose the parameters q, B_{Tleg}, and F we consider the constraints imposed by the power required to produce the toroidal field using copper coils (P_{TF}), and by the power to drive the plasma current (P_{CD}). That is, we assume TF coil cooling is possible, and that there are no TF coil material strength problems. These assumptions advantage low-A, where they are more questionable. A working constraint is that the total auxiliary power required should be a (small) fraction of the total electric power of the reactor; we write the recirculating power fraction as (see *Figure 2*)

$$\chi = \frac{P_{TF}/f_{TF} + P_{CD}/f_{CD}}{P_{el}} = \frac{P_{TF}/f_{TF} + P_{CD}/f_{CD}}{f_{el} P_n} \tag{17}$$

where we have assumed specified efficiencies of conversion, f_{TF} and f_{CD}, from electricity to either P_{TF} or P_{CD}. We have also assumed that any additional heating $P_H = 0$, valid for the constraints of the analytic model.

In the following analysis we consider two limiting cases where $P_{CD} = 0$, namely completely efficient and completely inefficient auxiliary current drive. In the first case (completely efficient) then clearly $P_{CD} = 0$; the idea of using reflected radiation to drive the plasma current [16] is approximated by this assumption. In the second case (completely inefficient) then the only way to drive the plasma current is by a bootstrap effect. In this

case no auxiliary current drive is needed (or can be tolerated), so again $P_{CD} = 0$. Under these circumstances $F = 1$ defines ignition, and

$$\chi = \frac{P_{TF}}{f_{TF} f_{el} P_n} \tag{18}$$

We will show that, in the case where $P_{CD} = 0$, a restriction to B_{Tleg} is obtained by restricting χ. To specify χ requires invoking either a neutron wall loading limit, or a beta limit. Concerning restrictions on q, there are two possibilities. First, if auxiliary current drive is completely efficient, we can choose any $q > q_{min}$, where we take $q_{min} = 3.2$. Secondly, if auxiliary current drive is completely inefficient, then we must rely on bootstrap current. In this case the requirement that $f_{bs} = 1$ and a knowledge of the beta limits defines q. While such operation is unlikely, it places a simple bound on the machine architecture and allows analytic scalings to be found. These restrictions (on current drive efficiency) are relaxed in Part II, to be published later; it is then found that reasonable-to-optimistic current drive efficiencies lead to values of major radius approximately half way between the two analytic limits considered here (see Appendix 2).

The conversion efficiency from neutron power P_n to electric power P_{el} is given by a futuristic $f_{el} = 0.4$ for that part of the surface area S covered with a nuclear breeding blanket. This assumes that the neutron wall loading is poloidally symmetric; numerical calculations find any wall loading asymmetry to be typically < 30%, and approximately independent of A [25]. Because we have utilized no inner blanket to obtain low-A, but rather utilized the space for the copper TF coil, the overall conversion efficiency is reduced from 0.4, and can be approximated by (see Appendix 1)

$$f_{el} \approx 0.4\left(\frac{1}{2} + \frac{\kappa^{0.13}}{\pi A}\right)\left(1 + 0.3\delta\kappa^{-0.5}\right) \tag{19}$$

This assumption advantages low A over normal A.

3.3.1.1. TF Coil Power

No inner equatorial nuclear shield is considered; easy TF coil replacement is assumed. For a central TF leg of height $2\kappa a$ and radius at the equator $R_0 - a$, the power consumed in producing the toroidal field is approximated by

$$P_{TF} = \frac{8\eta\pi\kappa B_{Tleg}^2 R_0}{\mu_0^2 f_{Cu} A}\left(1 - e^{-1.3\omega\sqrt{A-1}}\right) \tag{20}$$

where (see Appendix 1)

$$\omega = \left(1+\frac{2}{3}\delta\right) / \left(1-\frac{2}{3}\delta\right) \tag{21}$$

The power consumption in the outer TF legs is assumed negligible, because they can be made with as large a cross section as is necessary. The parameter f_{Cu} is the fraction of the TF leg area (assumed independent of height) made of conductor, the remaining fraction being used for cooling. We assume f_{Cu} = 0.7. The function $\left(1-e^{-1.3\omega\sqrt{A-1}}\right)$ describes the reduced TF leg resistance possible if the full aperture is used (hereafter called a 'Didcot' TF leg); $\omega = 1$ for a plasma with an elliptic cross section, and $\omega = \infty$ (any value > 1 is a sufficiently good approximation) for a triangular plasma with $\delta = 1$. We further assume that it is possible to remove the heat generated in the TF leg by water cooling, and that in so doing the resistivity $\eta \approx 2\text{x}10^{-8}$ Ω-m. We do not consider the power required to pump the cooling water.

3.3.1.2. Auxiliary Plasma Current Drive Power

The plasma current I_p required for equilibrium and confinement must be produced by non-inductive means because of the preferred steady state operation, and the lack of space for any inductor. The power P_{CD} required is written as

$$P_{CD} = \frac{\langle n \rangle R_0}{\eta_{CD}} I_{CD} = \frac{\langle n \rangle R_0}{\eta_{CD}} I_P (1 - f_{bs}) \tag{22}$$

with a dependence on volume averaged density $\langle n \rangle$ such that low density plasmas have a higher driven current for a given power. To avoid explicitly involving density as a parameter, we can replace the density with the fraction f_n of the Greenwald limit $(\bar{n} / 10^{20})\max = I_p(MA)/(\pi a^2)$, with $\bar{n}$ the line of sight averaged density:

$$f_n = \frac{\bar{n} / 10^{20}}{I_p / \left(10^6 \pi a^2\right)} = \frac{10^{-14} \pi \bar{n} R_0^2}{I_p A^2} = \frac{10^{-14} \pi \langle n \rangle R_0^2}{I_p A^2} \left[\frac{\sqrt{\pi}(1+\gamma_n)\Gamma(1+\gamma_n)}{2\left(\Gamma(3/2+\gamma_n)\right)} \right] \tag{23}$$

so that

$$P_{CD} = \frac{2x10^{14} \pi^{-3/2} \left(\Gamma(3/2+\gamma_n)\right)}{(1+\gamma_n)\Gamma(1+\gamma_n)} \frac{f_n A^2 I_p^2 (1 - f_{bs})}{\eta_{CD} R_0} \tag{24}$$

where the term in [ ] in Equation (23) including gamma functions converts between line averaged and volume averaged densities. Written in terms of the parameters considered as variables, namely B_{Tleg}, q, R_0, κ, and δ, this becomes

$$P_{CD} = \frac{2\sqrt{\pi} 10^{14} \left(\Gamma(3/2+\gamma_n)\right)}{\mu_0^2 (1+\gamma_n)\Gamma(1+\gamma_n)} \frac{B_{Tleg} R_o f_n (1 - f_{bs})}{q^2 \eta_{CD}} \frac{(A-1)^2 \left(1.22 - \frac{0.68}{A}\right)^2}{A^4 \left(1 - \left(\frac{1}{A}\right)^2\right)^4} \left(1 + \kappa^2 \left(1 + 2\delta^2 - 1.2\delta^3\right)\right)^2 \tag{25}$$

The bootstrap fraction f_{bs} is written as

$$f_{bs} \approx \alpha_{bs} \frac{\beta_p}{\sqrt{A}} = \frac{2\alpha_{bs} \beta_T q^2 (1+\kappa^2)}{\left(1 + \kappa^2 \left(1 + 2\delta^2 - 1.2\delta^3\right)\right)^2} \frac{A^{3/2} \left(1 - \left(\frac{1}{A}\right)^2\right)^4}{\left(1.22 - \frac{0.68}{A}\right)^2} \tag{26}$$

where the poloidal beta value is

$$\beta_p \equiv \frac{4\pi^2 a^2 \left(1+\kappa^2\right)\langle p\rangle}{\mu_0 I_p{}^2} \tag{27}$$

and the suitably averaged poloidal field is given by

$$B_p^2 = \left(\frac{\mu_0 I}{2\pi a}\right)^2 \frac{2}{\left(1+\kappa^2\right)} \tag{28}$$

For normal-A devices, with peaked current density profiles and edge-to-central safety factor ratios $q_a/q_0 > 1.5$, values $\alpha \approx 2$ are possible [26]. However we are interested in low-A with large bootstrap fractions, which necessitate hollow current density profiles; the current is driven in the region of pressure gradient. Note that operating low-A at low q also requires hollow current density profiles. With $q = 3.2$ at the edge the delineating aspect ratio between peaked and necessarily hollow current density profiles is that aspect ratio for which the current density profile is flat and central $q_0 = 1$, i.e. where $q_{cyl} \approx 1$ (Equation 8) and $A \approx 1.4$.

By comparing predictions of a 1-D spreadsheet (which calculates the bootstrap fraction based on the equations of Hirshman [27]) with various optimized advanced tokamak scenarios, Table 2 shows that a generous estimate is $\alpha_{bs} \approx 1$. The average coefficient for the normal aspect ratio cases is $\overline{\alpha}_{bs} = 0.6 \pm 0.2$, while for the low aspect ratio cases it is $\overline{\alpha}_{bs} = 0.76 \pm 0.02$.

Table 2. Bootstrap fractions of projected devices

Device	A	κ	f_{bs}	$\beta_{pa}/\sqrt{A}$	α_{bs}
TPX[28]	4.5	1.95	0.93	1.35	0.69
Reactor SS[3]	4.0	1.80	0.87	2.34	0.37
Reactor FS[3]	4.0	1.60	0.57	0.77	0.74
Reactor PU[3]	4.0	1.60	0.34	.63	0.54
Reactor RS[3]	3.5	1.80	0.88	1.05	0.84
NSTX[29]	1.25	2.00	0.77	0.97	0.79
NSTX[30]	1.25	2.20	0.81	1.06	0.76
Reactor LAR[3]	1.25	2.20	0.79	1.06	0.75
Reactor STREAC19[6]	1.25	3	1.00	1.35	0.74

In the limiting case where $f_{bs} = 1$ the bootstrap current requirement can now be considered to supply a constraint on q, namely (see Equation (26))

$$q^2 = \frac{\left(1+\kappa^2\left(1+2\delta^2-1.2\delta^3\right)\right)^2}{2\beta_T\left(1+\kappa^2\right)} \frac{\left(1.22-\frac{0.68}{A}\right)^2}{A^{3/2}\left(1-\left(\frac{1}{A}\right)^2\right)^4} \tag{29}$$

3.3.1.3. Wall Loading

Tokamak reactors suffer from large power fluxes to material surfaces. The general problem is characterized by the power carried by the neutrons per unit first-wall area, or *wall loading*. This ratio is calculated using the surface area (see Appendix), $S \approx 2\pi^2 R_0 a(1+\kappa)\left(1-0.13\delta\kappa^{0.25}A^{-1}\right)$, which is the appropriate first-wall area for large A where a blanket surrounds the plasma. At low A there is no blanket at the inner equator, and the area of a spherical shell could be more appropriate. However, because the area associated with the inner major-radial wall becomes vanishingly small as $A \rightarrow 1$, the error introduced by using the elliptical version is small.

Material availability restricts the possible neutron power per unit area to values

$$P_n = \Gamma_n S \tag{30}$$

where $\Gamma_n < 5$ to 10 MWm^{-2}. This, together with the surface area S, imposes a maximum neutron power P_n. By further imposing a value of χ, (Equation (18)) and utilizing Equation (20) for P_{TF}, a constraint on B_{Tleg} is implied.

3.3.1.4. Beta Limits

An alternate restriction to the maximum possible neutron power is a beta limit. Two cases are considered, namely an absolute beta and a normalized beta restriction. We use the definition $\beta_T = 4\mu_0 k_b g_2 \langle nT \rangle / B_{T0}^2$ (k_b is Boltzmann's constant), that is, with respect to the applied toroidal field, on axis, in vacuum. At low-A the correct volume averaged total field is larger than B_{T0}, and the total beta (with respect to the volume averaged total field) can be as small as half that quoted here.

The neutron power ($P_n \approx 4P_\alpha$) from Equation (2) expressed in terms of β_T is

$$P_n = 1.83\times10^{7}\beta_T^2 B_{Tleg}^4 R_0^3 \kappa f_2(\delta,A)\frac{(A-1)^4}{A^6}\frac{g^2\left(1+\gamma_n+\gamma_T\right)^2}{g_2^2\left(1+2\left(\gamma_n+\gamma_T\right)\right)} \tag{31}$$

By imposing a restriction to the absolute $\beta_T < \beta_{Tmax}$ we restrict P_n, and through Equation (18), Equation (20) and Equation (31) obtain a relationship between B_{Tleg} and R_0; that is, a restriction on B_{Tleg}.

A normalized beta limit is usually more appropriate. In this case we assume that a limiting value of β_T exists, which can be written as [19]

$$\beta_T \le 10^{-8}\beta_N \frac{I_p(\mathrm{A})}{a(\mathrm{m})B_{T0}(\mathrm{T})}, \tag{32}$$

Then using Equation (7), Equation (8), Equation (31) and Equation (32) the neutron power can be written as

$$P_n \le 1.14\times10^{4}\frac{\beta_N^2 B_{Tleg}^4 R_0^3}{q^2}\kappa\left(1+\kappa^2\left(1+2\delta^2-1.2\delta^3\right)\right)^2 f_2(\delta,A)\frac{\left(1.22-\dfrac{0.68}{A}\right)^2}{(1+A)^4}\frac{g^2\left(1+\gamma_n+\gamma_T\right)^2}{g_2^2\left(1+2\left(\gamma_n+\gamma_T\right)\right)} \tag{33}$$

Using this expression together with Equation (18) and Equation (20) provides a relationship between B_{Tleg} and R_0, that is, a restriction on B_{Tleg}.

There is one further constraint, imposed by the analytic model used for the cross section (see *Figure 3*). Because this approximation is only good for $T \lesssim 25$ keV, and because there is a maximum density limit attainable (the Greenwald density limit, Equation (23), with $f_n < 1$), there is an additional beta limit. Rather than derive expressions for the machine architecture associated with this limit, checks are imposed after a particular device is designed to ensure that this limit is not exceeded, namely that

$$\beta_T \le \beta_{gw} = \frac{8x10^{14}\pi^{-3/2}\mu_0 k_b g_2 \Gamma\left(3/2+\gamma_n\right)T_{0,\max}}{\left(1+\gamma_n+\gamma_T\right)\Gamma\left(1+\gamma_n\right)}\frac{I_p A^2}{B_{T0}^2 R_0^2} \tag{34}$$

where $T_{0,\max}$ is the maximum value of T on axis which is consistent with the fitting. Values for I_p and B_{T0} in terms of the variables q and B_{Tleg} must be used (see Equation (7), Equation (8), and either Equation (9) or Equation (10)), so that (with Equation (10))

$$\beta_T \le \beta_{gw} = \frac{8x10^{14}\pi^{-1/2}k_b g_2 \Gamma(3/2+\gamma_n)T_{0,\max}}{(1+\gamma_n+\gamma_T)\Gamma(1+\gamma_n)B_{Tleg}R_0 q} \frac{A\left(1.22-\dfrac{0.68}{A}\right)}{(A-1)\left(1-\left(\dfrac{1}{A}\right)^2\right)^2}\left(1+\kappa^2\left(1+2\delta^2-1.2\delta^3\right)\right)$$

(34a)

q is taken as either q_{min} or given by the restriction $f_{bs} = 1$ (Equation (29)).

3.3.2. Superconducting TF coils

Although this paper is primarily concerned with normal copper TF coils, we compare the results with those for a superconducting system. For a superconducting TF system an inner shield $w_b \approx 1$ m must be used, so that Equation (15) is relevant. As in the normal copper case, there are three parameters which must be further constrained, namely the safety factor q, the magnetic field at the TF leg B_{Tleg}, and F.

In the superconducting case we take B_{Tleg} a constant (e.g. 13 T) and ignore the TF power requirements, so that $P_{TF} = 0$. Concerning auxiliary plasma current drive, the same two limiting cases as discussed previously can be solved, namely completely efficient and completely inefficient auxiliary drive. For the completely efficient current drive, the smallest superconducting TF case is approximated using Equation (15), with $q = q_{min}$ (taken as 3.2) and $B_{Tleg} = 13$ T, and (because $P_{CD} = P_{TF} = 0$) $F = 1$. For the completely inefficient current drive, 100% bootstrap plasma current must be considered ($f_{bs} = 1$) which imposes a relation between q and β; again $P_{CD} = 0$. In both cases the recirculating power is not a relevant parameter.

In this way closed expressions are determined for the smallest superconducting device. The output power is determined by the neutron power, given by Equation (30) (wall loading), Equation (31) (absolute beta), Equation (33) (normalized beta), or Equation (34) (Greenwald limit). When dealing with superconducting devices there are two further modifications. First, wherever B_{Tleg} appears it must be replaced by $B_{Tleg}\left(1-w_b A/R_0(A-1)\right)$ to allow for the inner shield. Second, because of the inner shield, the conversion efficiency from neutron power to electric power is taken as $f_{el} = 0.4$, independent of plasma geometry.

3.4. Analytic Results - Copper TF Coils

Here we present the analytic formulae relevant for devices with normal copper toroidal field coils, together with graphical examples which depict the scaling of major radius with aspect ratio. For these graphs we use the nominal values listed in Table 3, which also includes values used when considering superconducting coils. The values chosen are intended to be representative of those used in the various studies which were summarized in Table 1. Variations in certain parameters, in particular the recirculating power fraction χ, wall loading Γ_n, β_N, and β_T, will be considered.

Table 3. Values used in determining variations of major radius with A.

Parameter	Superconducting TF	Normal Cu TF
α_a	-0.37	-0.37
α_R	1.75	1.75
c	4.778×10^{-5}	4.778×10^{-5}
H	2	2
Z_i	6	6
Z_{eff}	1.5	1.5
γ_n	1	1
γ_T	1	1
κ	2	2
δ	0.3	0.3
f_{TF}		0.8
f_{el}	0.4	$0.4\left(0.5+\kappa^{0.13}/(\pi A)\right)\left(1+0.3\delta\kappa^{-0.5}\right)$
f_{Cu}		0.7
B_{Tleg} (T)	13	defined by restriction to χ
q	3.2, or defined by $f_{bs} = 1$	3.2, or defined by $f_{bs} = 1$
χ	0.31, 0.62	0.31, 0.62
β_N	3, 5	3, 5
β_T	0.5, 1	0.5, 1
Γ_n (Wm^{-2})	2×10^6, 5×10^6	2×10^6, 5×10^6

3.4.1. Completely Efficient Auxiliary Current Drive ($\eta_{CD} = \infty$)

In this case we are free to choose any $q > q_{min}$, which is taken later as 3.2. There are then two equations to be solved, for R_0 and B_{Tleg}.

3.4.1.1. Wall Loading Limit

Using the concepts discussed in Section 3.3.1.3, together with Equation (16), we obtain unique expressions for B_{Tleg} and R_0 of the smallest device limited by wall loading, in terms of the recirculating power fraction χ, namely

$$B_{Tleg,\Gamma} = \left[\frac{\mu_0^2 \pi \chi f_{TF} f_{el} f_{Cu} \Gamma_n}{4\eta\left(1 - e^{-1.3\omega\sqrt{A-1}}\right)} \frac{(1+\kappa)\left(1 - 0.13\delta\kappa^{0.25}A^{-1}\right)}{\kappa} \left(\frac{q^2 f_2(\delta, A)}{\lambda f_1(A) f_3(\delta, \kappa)} \right)^{\frac{1}{2\alpha_R + 2\alpha_a - 1}} \right]^{\frac{2\alpha_R + 2\alpha_a - 1}{4\alpha_R + 4\alpha_a}} \tag{35}$$

and

$$R_\Gamma = \left[\frac{1.92x10^{-6} \pi g_2^2 \eta\left(1 - e^{-1.3\omega\sqrt{A-1}}\right) q^2 \left(1 + 2(\gamma_n + \gamma_T)\right) \kappa f_2(\delta, A)}{\mu_0^2 \chi f_{TF} f_{el} f_{Cu} \Gamma_n c^2 H^2 g^2 \left(1 + \gamma_n + \gamma_T\right)^2 f_1(A) f_3(\delta, \kappa)(1+\kappa)\left(1 - 0.13\delta\kappa^{0.25}A^{-1}\right)} \right]^{\frac{1}{2\alpha_R + 2\alpha_a}} \tag{36}$$

For typical values of α_a and α_R we find $B_{Tleg,\Gamma} \propto (\chi\Gamma_n)^{0.32}$, i.e. the toroidal magnetic field can be increased and a smaller machine built if a higher recirculating power fraction (χ), or higher wall loading (Γ_n), is permitted. Also $R_\Gamma \propto \left[q^2 / \chi\Gamma_n H^2\right]^{0.36}$. That is, increasing the allowed recirculating power fraction χ, wall loading Γ_n, or confinement factor H, or decreasing the allowed safety factor q, allows a smaller machine to be built. *Figure 4* shows R_Γ as a function of A, for two values of χ and Γ_n. R_Γ decreases with decreasing A, showing that smaller devices are possible at low A than at normal A in this limit of completely efficient current drive efficiency.

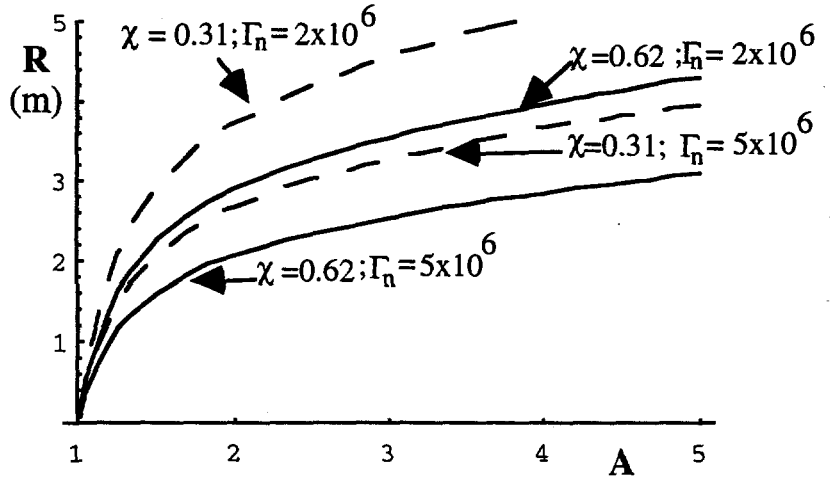

Figure 4. The major radius R_Γ of a wall-loading-limited device, with completely efficient current drive, as a function of aspect ratio A. Values of recirculating power fraction χ and wall loading Γ_n (in Wm^{-2}) are indicated; other values used are found in Table 3.

3.4.1.2. Absolute β Limit

Using the results discussed in Section 3.3.1.4, together with Equation (16), we obtain the expressions for B_{Tleg} and R_0 of the smallest device, limited by an absolute beta β_T, in terms of the recirculating power fraction χ:

$$B_{Tleg,\beta} = \left[\frac{8.7x10^5 \eta \left(1 - e^{-1.3\omega\sqrt{A-1}}\right) A^5}{\beta_T^2 \chi f_{TF} f_{el} f_{Cu} \dfrac{g^2(1+\gamma_n+\gamma_T)^2}{g_2^2(1+2(\gamma_n+\gamma_T))} (A-1)^4 f_2(\delta,A)} \left(\frac{\lambda f_1(A) f_3(\delta,\kappa)}{q^2 f_2(\delta,A)} \right)^{\frac{2}{2\alpha_R+2\alpha_a-1}} \right]^{\frac{2\alpha_R+2\alpha_a-1}{4\alpha_R+4\alpha_a-6}} \tag{37}$$

The associated major radius R_β is found as

$$R_\beta = \left[\frac{8.7x10^{13} \eta c^2 H^2 f_1(A) \left(1 - e^{-1.3\omega\sqrt{A-1}}\right) A^5 f_3(\delta,\kappa)}{48\pi^2 q^2 \beta_T^2 \chi f_{TF} f_{el} f_{Cu} (A-1)^4 \left(f_2(\delta,A)\right)^2} \right]^{\frac{1}{3-2\alpha_R-2\alpha_a}} \tag{38}$$

For typical values of α_a and α_R we find $R_\beta \propto \left[H^2 / q^2 \beta_T^2 \chi\right]^{4.17}$. Therefore increasing the maximum allowed β_T decreases the machine size, as does increasing the safety factor q or decreasing the confinement factor H. Thus R_β and R_Γ have very different dependencies on H and q. *Figure 5* show $R\beta$ as a function of A, for different χ and β_T Note that the horizontal scale is different from *Figure 4.*; in *Figure 5* we concentrate on low A. We see

that restricting the absolute β_T value imposes a lower A limit. At larger A, if β_T was the only restriction, very small device could be operated.

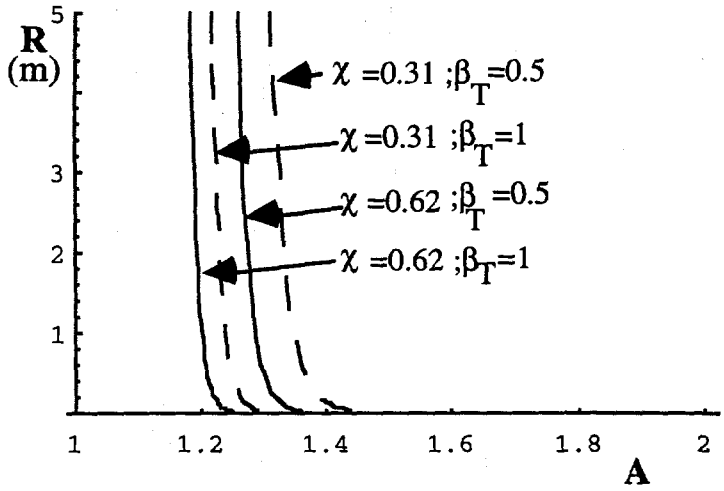

Figure 5. The major radius $R\beta$ of a β_T limited device, with completely efficient current drive, as a function of aspect ratio A. Values of recirculating power fraction χ and absolute beta β_T are indicated; other values are found in Table 3.

3.4.1.3. Normalized β Limit

Using the results discussed in section 3.3.1.4, together with Equation (16), we obtain the expressions for B_{Tmax} and R_0 of the smallest device, limited by a normalized beta, in terms of the recirculating power fraction χ:

$$B_{Tleg,\beta N} = \left[\frac{1.39x10^{9}\eta\left(1-e^{-1.3\omega\sqrt{A-1}}\right)q^{2}A^{7}(A-1)^{-4}\left(1-\left(\frac{1}{A}\right)^{2}\right)^{4}\left(\frac{\lambda f_1(A)f_3(\delta,\kappa)}{q^{2}f_2(\delta,A)}\right)^{\frac{2}{2\alpha_R+2\alpha_a-1}}}{\beta_N^{2}\chi f_{TF}f_{el}f_{Cu}\frac{g^{2}\left(1+\gamma_n+\gamma_T\right)^{2}}{g_2^{2}\left(1+2\left(\gamma_n+\gamma_T\right)\right)}\left(1.22-\frac{0.68}{A}\right)^{2}\left(1+\kappa^{2}\left(1+2\delta^{2}-1.22\delta^{3}\right)\right)^{2}f_2(\delta,A)} \right]^{\frac{2\alpha_R+2\alpha_a-1}{4\alpha_R+4\alpha_a-6}} \tag{39}$$

The associated major radius $R_{\beta N}$ is found by substitution of Equation (39) into Equation (16):

$$R_{\beta N} = \left[\frac{1.39x10^{17}\eta c^{2}H^{2}\left[\left(1-e^{-1.3\omega\sqrt{A-1}}\right)A^{7}(A-1)^{-2}A^{-(4+2\alpha_a)}\right]}{48\pi^{2}\beta_N^{2}\chi f_{TF}f_{el}f_{Cu}\left(f_2(\delta,A)\right)^{2}} \right]^{\frac{1}{3-2\alpha_R-2\alpha_a}} \tag{40}$$

That is, for typical values of α_R and α_a, $R_{\beta N} \propto \left(H^2 / \beta_N \chi\right)^{4.17}$: increasing β_N or χ reduces machine size, but increasing H increases machine size. Note that $R_{\beta N}$ is the only one of the three restricted major radii considered so far that is independent of q; therefore the same expression will apply to a β_N-restricted machine with 100% bootstrap (obtained by operating at high q). *Figure 6* illustrates the dependence of $R_{\beta N}$ on A for different values of β_N and χ, other values used are listed in Table 3. As for the β_T limit, the β_N limit imposes a value of A below which a device cannot be operated. However, it also imposes a high-A restriction. For the example shown with $\chi = 0.31$ and $\beta_N = 3$ the β_N -limited R shows a clear minimum with $A \approx 2$. As either χ or β_N is increased the minimum becomes broader, i.e. less sensitive to the value of A, illustrating one advantage of increasing β_N.

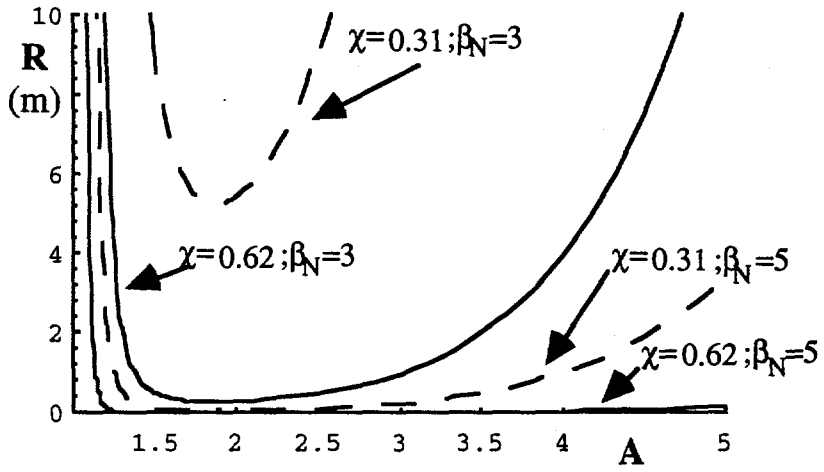

Figure 6. The major radius $R_{\beta N}$ of a β_N limited device, with completely efficient current drive, as a function of aspect ratio A. Values of χ and β_N are indicated; other values used are found in Table 3.

This section is summarized by noting that the major radius of the smallest device with copper TF coils and completely efficient current drive is given by the largest of the three values so far considered, namely R_β, $R_{\beta N}$ and R_Γ. The results are shown in *Figure 7* for χ = 0.31 and 0.62, β_N = 3 and 5, and the maximum β_T = 1; other conditions are given in Table 3. Note that β_T = 1 corresponds to a true total beta value ≈ 0.5 at low A, where β_T is large. In all cases the accessibility of low A is restricted either by the β_N or the β_T limit. For small χ (= 0.31) and small β_N (= 3) the β_N limit is restricting throughout the A-range, and there are obvious gains in producing a smaller device by utilizing low A. However if β_N is increased from 3 to 5, with χ maintained at 0.31, then the wall loading limit applies over the A range considered (except at the lowest A). If χ is now increased from 0.31 to 0.62 then wall loading limits over most of the A-range considered (except at the lowest and highest A's).

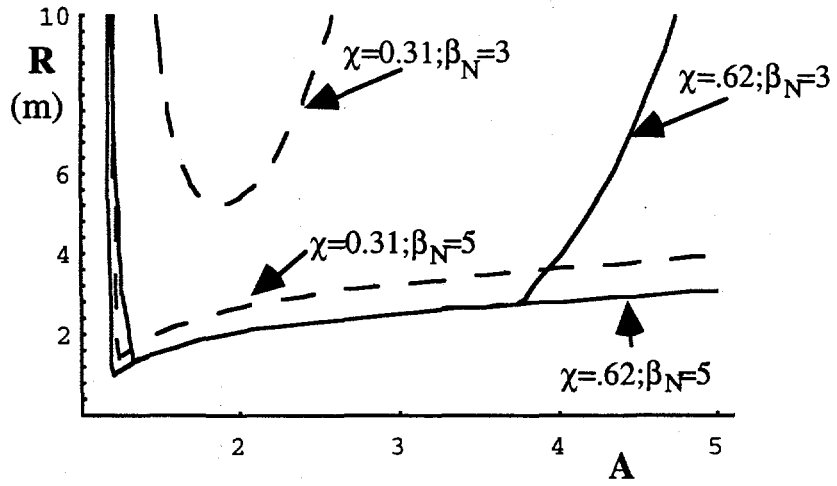

Figure 7. The major radius of the smallest device, considering β, β_N and Γ_n limits, for χ = 0.31 and 0.62, β_N = 3 and 5, other conditions as given in Table 3.

The variation of toroidal field at the inner leg with A can also be derived, as the minimum of the three values discussed ($B_{Tleg,\Gamma}$, $B_{Tleg,\beta}$ and $B_{Tleg,\beta N}$). The results are shown in *Figure 8*. Increasing χ allows higher fields; increasing β_N removes the limit appearing at higher A. With the parameter values chosen the maximum fields required (≈ 12 T) are very reasonable.

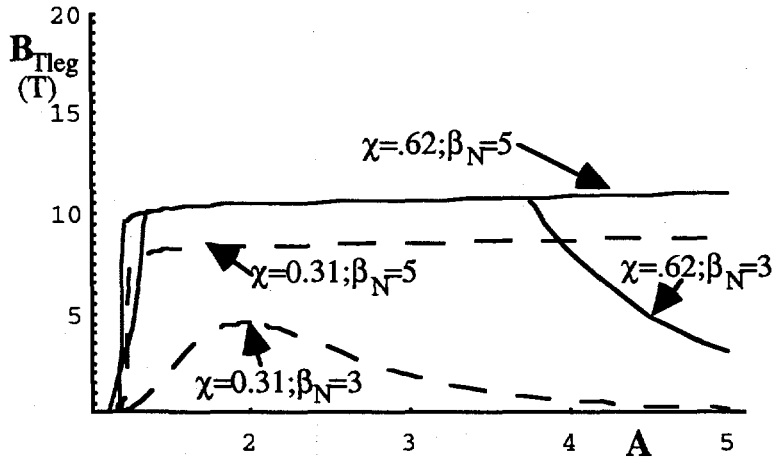

Figure 8. The magnetic field at the surface of the toroidal field leg, corresponding to the cases considered in *Figure 7*.

The required plasma currents (I_p) are deduced using the analytic expressions for the different R's and B_{Tleg}'s in Equation 7, and results are shown in *Figure 9*. Any gains (in allowing smaller devices) at low A are achieved at the expense of requiring large plasma currents, and so far no account has been taken of the current drive efficiency. Only at the lower χ and lower β_N do the curves become distinguishable. This is because under these

circumstances the largest plasma current is determined by the β_N limit; increasing either β_N or χ ensures that the maximum plasma current is determined by the wall loading limit.

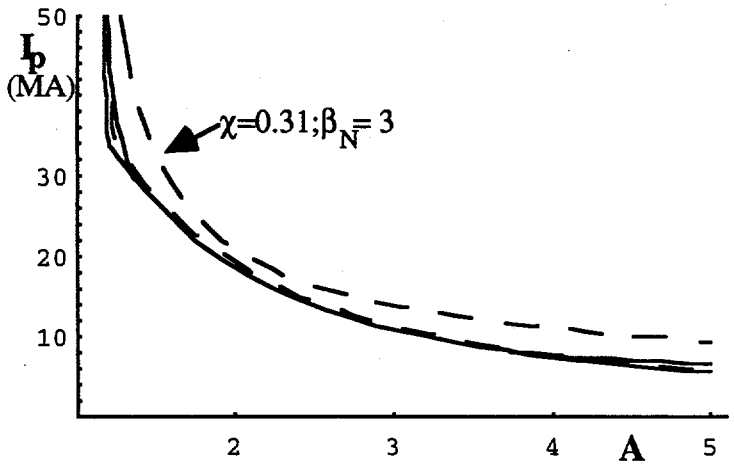

Figure 9. The plasma currents I_p corresponding to the cases considered in *Figure 7* and *Figure 8.*

3.4.2. Completely Inefficient Auxiliary Current Drive ($\eta_{CD} = 0$)

3.4.2.1. Wall Loading Limit

This will turn out to be the most interesting case. The toroidal beta value β_T appears in Equation (29) for the bootstrap current fraction f_{bs}. When β_T is restricted by wall loading, we obtain from the definition of wall loading (Equation (30)) and from the neutron power (Equation (31)) the expression

$$\beta_T = \left[\frac{2\pi^2}{1.83\times 10^7} \frac{\Gamma_n}{R_0 B_{Tleg}^4} \frac{A^5}{(A-1)^4} \frac{(1+\kappa)\left(1-0.13\delta\kappa^{0.25}A^{-1}\right)}{\kappa f_2(\delta,A)} \frac{g_2^2\left(1+2\left(\gamma_n+\gamma_T\right)\right)}{g^2\left(1+\gamma_n+\gamma_T\right)^2} \right]^{\frac{1}{2}} \quad (41)$$

Using Equation (41) in Equation (29) we obtain an expression for the safety factor required to obtain a given f_{bs}:

$$q^2 = \frac{1.51x10^3 f_{bs}}{\pi\sqrt{\Gamma_n}} \frac{\left(1.22-\frac{0.68}{A}\right)^2 (A-1)^2}{\left(1-\left(\frac{1}{A}\right)^2\right)^4 A^4} \sqrt{R_0} B_{Tleg}^2 \frac{\left(1+\kappa^2\left(1+2\delta^2-1.2\delta^3\right)\right)^2 \sqrt{\kappa}\sqrt{f_2(\delta,A)}}{\left(1+\kappa^2\right)\sqrt{(1+\kappa)\left(1-0.13\delta\kappa^{0.25}A^{-1}\right)}}$$

$$\times \frac{g\left(1+\gamma_n+\gamma_T\right)}{g_2\sqrt{\left(1+2\left(\gamma_n+\gamma_T\right)\right)}} \tag{42}$$

which we write as

$$q^2 = k_1\sqrt{R_0} B_{Tleg}^2 \tag{43}$$

where

$$k_1 = \frac{1.51x10^3 f_{bs}}{\pi\sqrt{\Gamma_n}} \frac{\left(1.22-\frac{0.68}{A}\right)^2 (A-1)^2}{\left(1-\left(\frac{1}{A}\right)^2\right)^4 A^4} \frac{\left(1+\kappa^2\left(1+2\delta^2-1.2\delta^3\right)\right)^2 \sqrt{\kappa}\sqrt{f_2(\delta,A)}}{\left(1+\kappa^2\right)\sqrt{(1+\kappa)\left(1-0.13\delta\kappa^{0.25}A^{-1}\right)}}$$

$$\times \frac{g\left(1+\gamma_n+\gamma_T\right)}{g_2\sqrt{\left(1+2\left(\gamma_n+\gamma_T\right)\right)}} \tag{44}$$

Now we have three equations to solve, for $B_{Tleg,}$, R_0 and q. We write the equations for $B_{Tleg,}$ (Equation (35)) and R_0 (Equation (36)) as

$$B_{Tleg,\Gamma} = k_2 q^{\left(\frac{1}{2\alpha_R+2\alpha_a}\right)} \tag{45}$$

where

$$k_2 = \left[\frac{\mu_0^2\pi\chi f_{TF} f_{el} f_{Cu}\Gamma_n}{4\eta\left(1-e^{-1.3\omega\sqrt{A-1}}\right)} \frac{(1+\kappa)\left(1-0.13\delta\kappa^{0.25}A^{-1}\right)}{\kappa} \left(\frac{f_2(\delta,A)}{\lambda f_1(A) f_3(\delta,\kappa)}\right)^{\frac{1}{2\alpha_R+2\alpha_a-1}}\right]^{\frac{2\alpha_R+2\alpha_a-1}{4\alpha_R+4\alpha_a}} \tag{46}$$

and

$$R_\Gamma = k_3 q^{\left(\frac{1}{\alpha_R+\alpha_a}\right)} \tag{47}$$

where

$$k_3 = \left[\frac{1.92x10^{-6}\pi\eta\left(1-e^{-1.3\omega\sqrt{A-1}}\right)g_2^2\left(1+2(\gamma_n+\gamma_T)\right)\kappa f_2(\delta,A)}{\mu_0^2\chi f_{TF}f_{el}f_{Cu}\Gamma_n c^2 H^2 g^2\left(1+\gamma_n+\gamma_T\right)^2 f_1(A)f_3(\delta,\kappa)(1+\kappa)\left(1-0.13\delta\kappa^{0.25}A^{-1}\right)} \right]^{\frac{1}{2\alpha_R+2\alpha_a}} \quad (48)$$

The solution to Equation (43) through Equation (48) is

$$R_{\Gamma bs} = \left[k_1 k_2^2 k_3^{2\alpha-1}\right]^{\frac{2}{(4\alpha-3)}} \propto H^{-1.6}\Gamma_n^{-0.4}\chi^0 \quad (49)$$

$$B_{Tleg,\Gamma bs} = \left[k_1 k_2^{(4\alpha-1)} k_3^{\frac{1}{2}}\right]^{\frac{1}{(4\alpha-3)}} \propto \chi^{0.5}\Gamma_n^{0.3}H^{-0.8} \quad (50)$$

$$q_{\Gamma bs} = \left[k_1 k_2^2 k_3^{\frac{1}{2}}\right]^{\frac{2\alpha}{(4\alpha-3)}} \propto \chi^{0.5}H^{-1.2} \quad (51)$$

where we have written

$$\alpha = \alpha_a + \alpha_R \quad (52)$$

That is, we have completely determined the smallest machine to operate with $f_{bs} = 1$, the smallest machine which needs no auxiliary current drive. The variations shown in Equations (49) through (51) are for the standard values α_R = 1.75 and α_a = -0.37. The major radius of the smallest device with f_{bs} = 1 is independent of the recirculating power fraction χ, but increasing χ increases $B_{Tleg,\Gamma bs}$ and $q_{\Gamma bs}$. This lack of a dependence of $R_{\Gamma bs}$ on χ means that the power to the grid, $P_{gr} = f_{el}P_n(1-\chi) = f_{el}S\Gamma_n(1-\chi)$, is controlled by changing χ, i.e. by changing $B_{Tleg,\Gamma bs}$. Increasing confinement (increasing H) decreases $R_{\Gamma bs}$, $B_{Tleg,\Gamma bs}$ and $q_{\Gamma bs}$. Increasing the permitted neutron wall loading Γ_n decreases $R_{\Gamma bs}$, but increases $B_{Tleg,\Gamma bs}$.

Figure 10 shows the scaling of R with A for the nominal values listed in Table 3, with Γ_n = 2x10^6 Wm^{-2} and 5x10^6 Wm^{-2}. Comparing the results with the cases for $\eta_{CD} = \infty$ (*Figure 4*) we find the major radius is now larger, and increases as A decreases. This is because the safety factor required to provide f_{bs} = 1 is very large at low A, as shown in *Figure 11*. However at normal A , q can reach the assumed lower limit (q > 3.2). Although R is not dependent on the recirculating power fraction, q is. That is, changing χ does not change the minimum device size, but does change the safety factor (and toroidal field). There is a very weak dependence of q on Γ_n which cannot be distinguished in *Figure 11*.

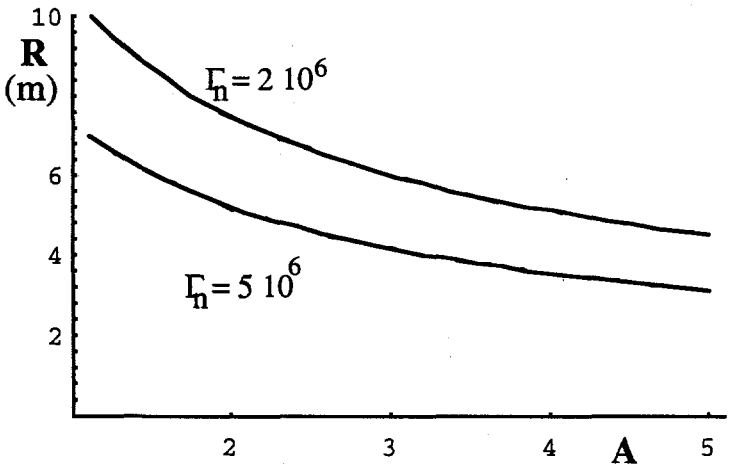

Figure 10. The device major radius R as a function of aspect ratio A for a fully bootstrap-driven case. The neutron wall loading $\Gamma_n = 2\text{x}10^6$ Wm^{-2} and $5\text{x}10^6$ Wm^{-2}; other parameters are found in Table 3.

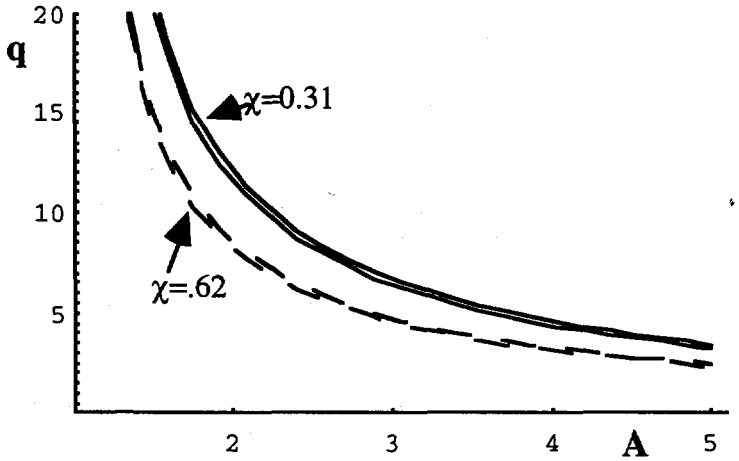

Figure 11. The safety factor q associated with operating with $f_{bs} = 1$, for the cases shown in *Figure 10.*

For completeness we show in *Figure 12* the toroidal field at the TF leg associated with the cases discussed above, and in *Figure 13* the associated plasma current I_p. It is not possible to distinguish the separate plasma currents. However the toroidal field at the TF leg increases with decreasing A, increasing wall loading, or increasing recirculating power. At the lowest A's considered, values $B_{Tleg} > 20$ T are required.

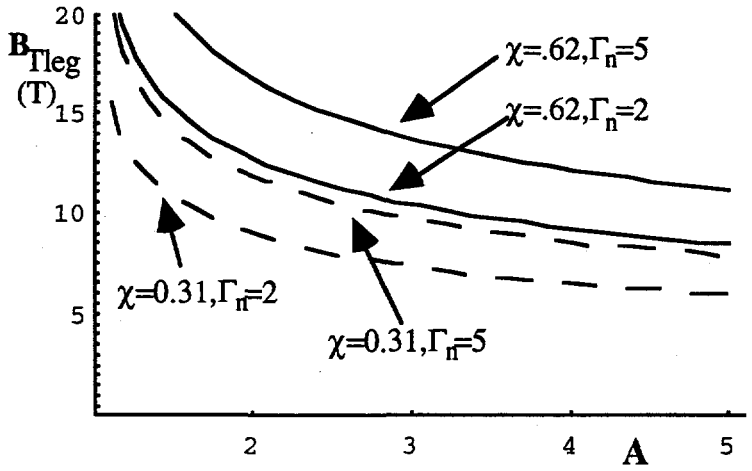

Figure 12. The toroidal field B_{Tleg} at the TF leg surface, for the conditions discussed in the text. Γ_n is given in MWm^{-2}.

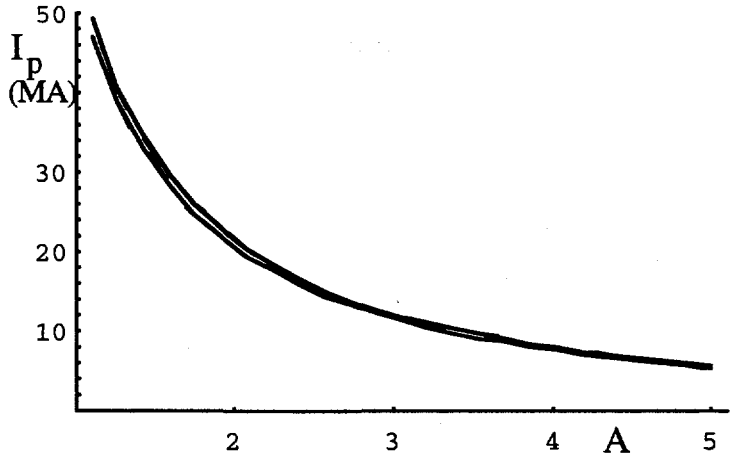

Figure 13. The plasma current I_p for the conditions discussed in the text.

3.4.2.2. Absolute β Limit

We require the three equation for R_0, q and B_{Tleg}. In the case of β_T limitations the safety factor is written as (see Equation 29)

$$q^2 = k_4 \beta_T^{-1} \tag{53}$$

where

$$k_4 = \frac{\left(1+\kappa^2\left(1+2\delta^2-1.2\delta^3\right)\right)^2}{2\left(1+\kappa^2\right)} \frac{\left(1.22-\frac{0.68}{A}\right)^2}{A^{3/2}\left(1-\left(\frac{1}{A}\right)^2\right)^4} \tag{54}$$

The equation for major radius (Equation (38)) is rewritten as

$$R_\beta = k_5 q^{\left(\frac{2}{2\alpha-3}\right)} \tag{55}$$

where

$$k_5 = \left[\frac{8.7x10^{13}\eta c^2 H^2 f_1(A)\left(1-e^{-1.3\omega\sqrt{A-1}}\right)A^5 f_3(\delta,\kappa)}{48\pi^2\beta_T^2\chi f_{TF} f_{el} f_{Cu}(A-1)^4\left(f_2(\delta,A)\right)^2}\right]^{\frac{1}{3-2\alpha_R-2\alpha_a}} \tag{56}$$

Substituting for q from Equation (53) into Equation (55) gives

$$R_{\beta bs} = k_5\left(k_4\beta_T^{-1}\right)^{\frac{1}{2\alpha-3}} \tag{57}$$

Then for typical values $R_{\beta bs} \propto \left(H^2/\chi\beta_T\right)^{4.17}$. The other equation (for $B_{Tleg,\beta bs}$ obtained by substitution for q from Equation (53) into Equation (37)) is not interesting, because we will find that the strong dependence of $R_{\beta bs}$ on A precludes operating in the β_T-limited regime.

Figure 14 depicts the A-scaling of the absolute beta limited major radius, for different χ and β_T. The two cases with $\chi = 0.31$, $\beta_T = 1$ and $\chi = 0.62$, $\beta_T = 0.5$ lie on top of each other. As for the cases with $\eta_{CD} = \infty$, the absolute beta limit can be considered to impose a lower-A limit to the smallest device.

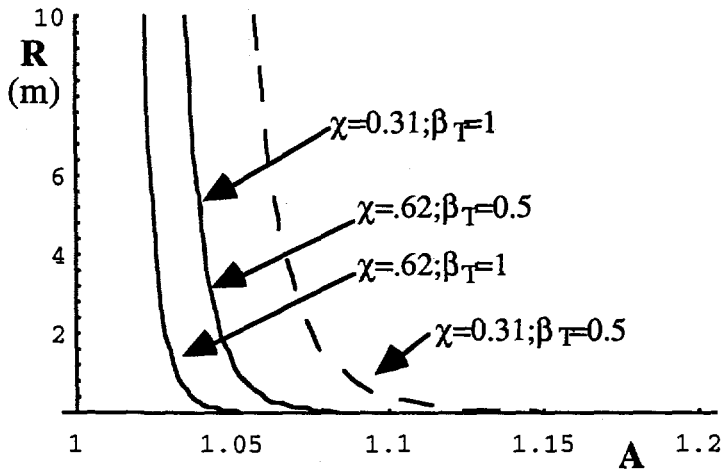

Figure 14. The major radius of the smallest absolute beta limited device, for $\chi = 0.31$ and 0.62, $\beta_T = 0.5$ and 1, as a function of aspect ratio A.

3.4.2.3. Normalized β Limit

The major radius $R_{\beta N}$ found previously (Equation (40)) is independent of q, and so is directly applicable to the $f_{bs} = 1$ case. That is,

$$R_{\beta Nbs} = \left[\frac{1.39x10^{17} \eta c^2 H^2 \left[\left(1 - e^{-1.3\omega\sqrt{A-1}}\right) A^7 (A-1)^{-2} A^{-(4+2\alpha_a)} \right]}{48\pi^2 \beta_N^2 \chi f_{TF} f_{el} f_{Cu} \left(f_2(\delta, A)\right)^2} \right]^{\frac{1}{3-2\alpha_R-2\alpha_a}} \tag{58}$$

That is, $R_{\beta Nbs} \propto \left(H^2 / \beta_N \chi\right)^{4.17}$; the dependence on A is as shown in *Figure 6*. To solve for $B_{Tleg\beta Nbs}$ and $q_{\beta Nbs}$ Equations (39) and Equation (29) (rewriting in terms of β_N from Equation (32), using also Equation (7) and Equation (8)) must be used. However, the results are not interesting, because we will find that the strong dependence of $R_{\beta Nbs}$ on A precludes operating in the β_N-limited regime.

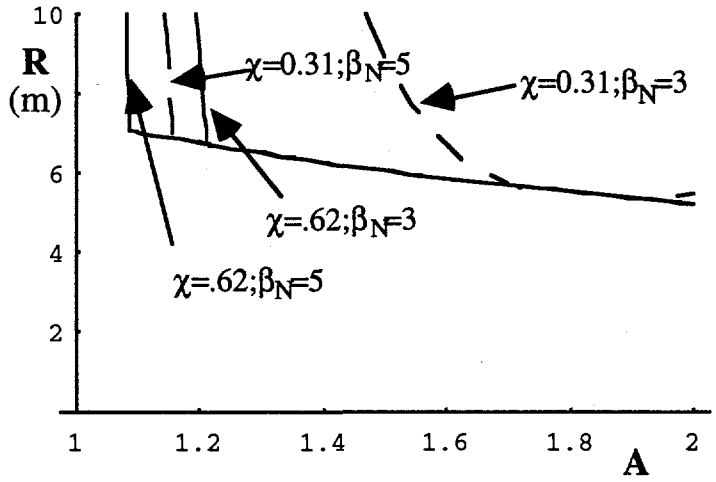

Figure 15. The major radius of the smallest device, allowing for normalized beta (β_N), absolute (β_T) and wall loading (Γ_n) limits to performance for a fully bootstrap-driven machine. Values used are $\chi = 0.31$ and 0.62, $\beta_N = 3$ and 5, $\Gamma_n = 5x10^6$ Wm^{-2}, and $\beta_T = 1$ (which is not restricting). Other values used are found in Table 3.

This section is summarized by noting that the major radius of the smallest device with copper TF coils and completely inefficient current drive is given by the largest of the three values so far considered, namely $R_{\beta bs}$, $R_{\beta N\, bs}$ and $R_{\Gamma bs}$. The results are shown in *Figure 15* for $\Gamma_n = 5x10^6$ Wm^{-2}, $\chi = 0.31$ and 0.62, $\beta_N = 3$ and 5, and the maximum $\beta_T = 1$, other conditions as given in Table 3. Note that $\beta_T = 1$ corresponds to a true total beta value ≈ 0.5 at low A, where β_T is large. However $\beta_T = 1$ is never limiting for the cases considered; the accessibility of low A is restricted by the β_N limit. For small χ (= 0.31)

and small β_N (= 3) the β_N limit is restricting throughout almost all the A-range. If β_N is increased from 3 to 5 then the wall loading limit (independent of χ) applies over almost all the A range considered (except at the lowest A).

3.5. Analytic Results - Superconducting TF coils

Here we use the concepts outlined in Section 3.3.2. Because the purpose of this paper is to discuss normal copper TF coils, we only provide the variations in major radius, and do not provide details of other parameters, such as I_p.

3.5.1. Completely Efficient Auxiliary Current Drive ($\eta_{CD} = \infty$)

In the case of completely efficient current drive we obtain Equation (15), with $F = 1$ and $q = q_{min}$. The power output is determined by either wall loading or β limits, but not the machine size, and $R_{sc} - R_{\min} \propto \left(q / HB_{Tleg}\right)^{1.14}$. The results apply only for $A > 1/\left(1 - w_b / R_{sc}\right)$. *Figure 16* shows the scaling of R_0 with A, for a realistic case with $w_b = 1$ m, and an unrealistic case with $w_b = 0$ m. This latter case can be considered as the smallest machine which can be built if neither plasma current nor toroidal field must be paid for. That is, it can be considered as the smallest device which could be used to study the physics of an ignited tokamak.

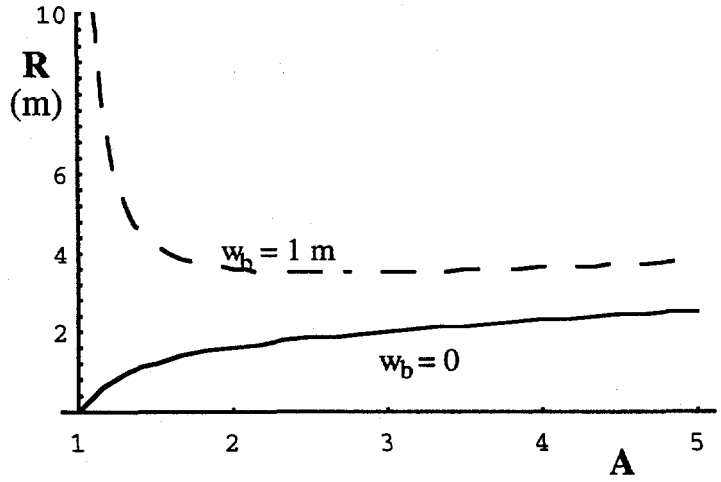

Figure 16. The major radius of the device in which the toroidal field and plasma current are not paid for. Broken line, with a 1 m blanket, and solid line, without a blanket. The safety factor $q = 3.2$, and the toroidal field at the toroidal field leg is 13 T. Other values used are found in Table 3.

3.5.2. Completely Inefficient Auxiliary Current Drive ($\eta_{CD} = 0$)

3.5.2.1. Wall Loading Limit

In the case of completely inefficient current drive we must restrict q by imposing $f_{bs} = 1$. In the case of wall loading limited operation (that which is generally applicable) then, from Equation (11) for R_0 and Equation (43) for q (with B_{Tleg} replaced by $B_{Tleg}\left(1 - w_b A/(R_0(A-1))\right)$ we obtain

$$R_{sc,\Gamma bs} = \left(k_6 k_1^{\frac{1}{2\alpha-1}} \right)^{\frac{4\alpha-2}{4\alpha-3}} \tag{59}$$

where

$$k_6 = \left(\frac{f_2(\delta, A)}{\lambda f_1(A) f_3(\delta, \kappa)} \right)^{\frac{1}{(2\alpha-1)}} \tag{60}$$

That is, $R_{sc,\Gamma bs} \propto \left(H^{-1.6}\Gamma_n^{-0.4}\right)$. Note that there is no dependence on recirculating power fraction χ, as in the normal copper case. No dependence on B_{Tleg} appears, although changing B_{Tleg} does change the power output to the grid. *Figure 17* shows the dependence of R on A for two values of Γ_n. Note that the analysis is only valid for $A > 1/\left(1 - w_b / R_0\right)$ ≈ 1.25 for the examples shown.

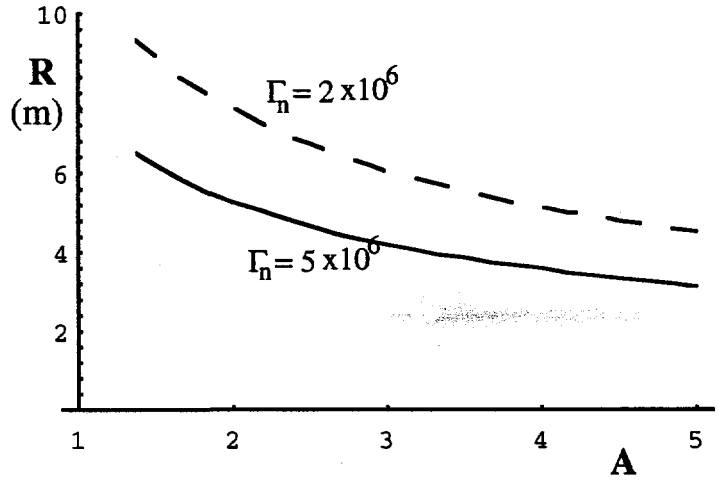

Figure 17. The major radius for a wall loading limited superconducting device, fully bootstrap-driven, with $\Gamma_n = 2\text{x}10^6$ Wm^{-2} (broken line) and $5\text{x}10^6$ Wm^{-2} (solid line). Other parameters are given in Table 3.

3.5.2.2. Absolute Beta Limit

In this case we utilize Equations (11) for R_0 and Equation (53) for q, and obtain

$$R_{sc,\beta bs} = k_6\left(\frac{k_4}{\beta_T}\right)^{\frac{1}{2\alpha-1}} B_{Tleg}^{-\frac{2}{2\alpha-1}} + \frac{w_b A}{A-1} \tag{61}$$

That is, $R_{sc,\beta bs} - R_{\min} \propto \left(\beta_T H^2 B_{Tleg}^2\right)^{-0.57}$. Figure 18 shows the A dependence for $\beta_T = 0.5$ and 1; there is little difference between the two cases. As in all other examples of β_T limiting cases discussed, an effective lower limit on A is imposed.

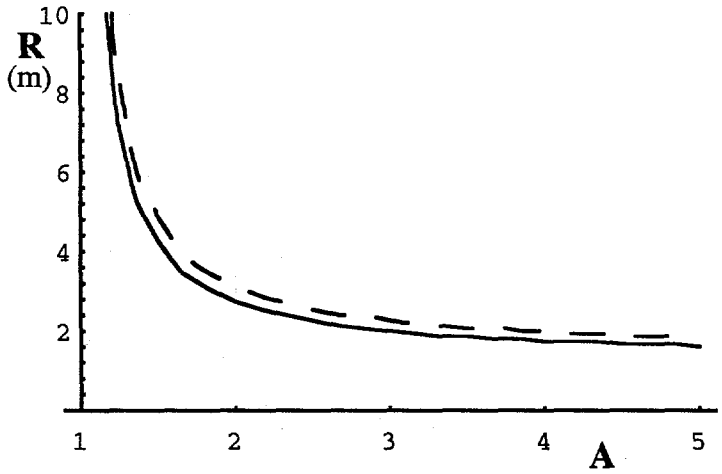

Figure 18. The major radius limited by absolute beta, for $\beta_T = 0.5$ (broken line) and 1 (solid line); other parameters are given in Table 3.

3.5.2.3. Normalized Beta Limit

We must derive an equation for q in terms of β_N. Using Equation 53, with β_T replaced by the maximum value predicted by Equation (32), we obtain

$$q = k_7 \tag{62}$$

where

$$k_7 = \frac{10^8 \mu_0 k_4 A\left(1-\left(\frac{1}{A}\right)^2\right)^2}{\pi\beta_N\left(1.22-\frac{0.68}{A}\right)\left(1+\kappa^2\left(1+2\delta^2-1.2\delta^3\right)\right)} \tag{63}$$

Utilizing Equations (11) for R_0, and Equation (62) for q, we obtain

$$R_{sc,\beta Nbs} = k_6\left(k_7\right)^{\frac{2}{2\alpha-1}} B_{Tleg}^{-\frac{2}{2\alpha-1}} + \frac{w_b A}{A-1} \tag{64}$$

That is, $R_{sc,\beta Nbs} - R_{\min} \propto \left(\beta_N H^2 B_{Tleg}^2\right)^{-0.57}$. *Figure 19* shows results for $\beta_N = 3$ and 5; the major radius increases as A decreases.

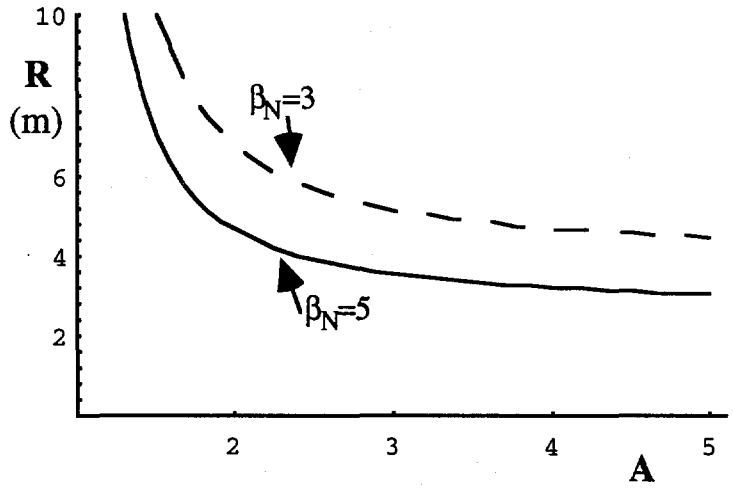

Figure 19. The major radius limited by β_N, for $\beta_N = 3$ and 5. Other parameters used are given in Table 3.

This section is summarized by noting that the major radius of the smallest device with superconducting TF coils and completely inefficient current drive is given by the largest of the three values so far considered, namely $R_{sc,\beta bs}$, $R_{sc,\beta Nbs}$ and $R_{sc,\Gamma bs}$. *Figure 20* shows results for $\beta_N = 3$ and 5, the maximum $\beta_T = 1$, and $\Gamma_n = 5\text{x}10^6\ \text{Wm}^{-2}$; other conditions as given in Table 3. Note that as discussed before $\beta_T = 1$ corresponds to a true total beta value ≈ 0.5 at low A, where β_T is large. However $\beta_T = 1$ is never limiting for the cases considered. The broken line ($\beta_N = 3$) is determined solely by the β_N -restricted radius. However as β_N is increased to 5 then the β_N limit only applies for $A < 1.6$; above this wall loading is the determining factor.

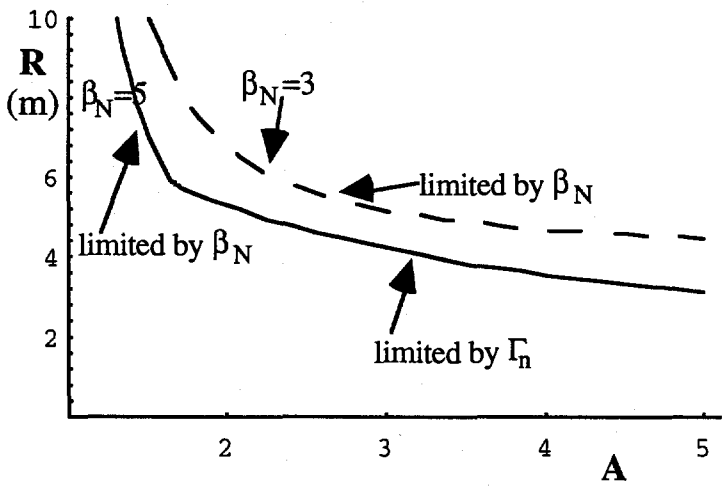

Figure 20. The major radius of the smallest device with a superconducting TF system, allowing for normalized beta (β_N), absolute (β_T) and wall loading (Γ_n) limits to performance for a fully bootstrap-driven machine. Values used $\beta_N = 3$ and 5, $\Gamma_n = 5\text{x}10^6$ Wm^{-2}, and $\beta_T = 1$ (which is not restricting). Other values used are found in Table 3.

3.6. Summary of Analytic Results, and Optimization

Table 4 is a summary of the equations derived for the smallest tokamak power plant under various conditions.

Table 4 Summary of equations for minimum major radius

	Normal Copper	**Normal Copper**	**Super-conducting**	**Super-conducting**
	$\eta_{CD} = 0$	$\eta_{CD} = \infty$	$\eta_{CD} = 0$	$\eta_{CD} = \infty$
wall loading	Equation (49)	Equation (36)	Equation (59)	Equation (15)
beta	Equation (57)	Equation (38)	Equation (61)	Equation (15)
normalized beta	Equation (58)	Equation (40)	Equation (64)	Equation (15)

Figure 21 shows results for both normal copper TF (solid line) and superconducting TF (broken line) for $\beta_N = 3.5$, $\Gamma_n = 5\text{x}10^6$ Wm^{-2}, for both the $f_{bs} = 1$ (completely inefficient current drive, R independent of χ) and for completely efficient current drive with $\chi = 0.62$. Also shown as a dotted line is the superconducting, completely inefficient case ($f_{bs} = 1$) with $\Gamma_n = 2\text{x}10^6$ Wm^{-2}. Considering first the superconducting cases, then although there is a small decrease in R as A is decreased in the completely efficient auxiliary current drive case, the machine encompassing volume V_m always increases as A is decreased

($V_m = 2\pi\kappa R_0^3 (A+1)^2 / A^3$). Considering the normal copper cases, only the completely efficient auxiliary current drive case exhibits a smaller R as A is decreased.

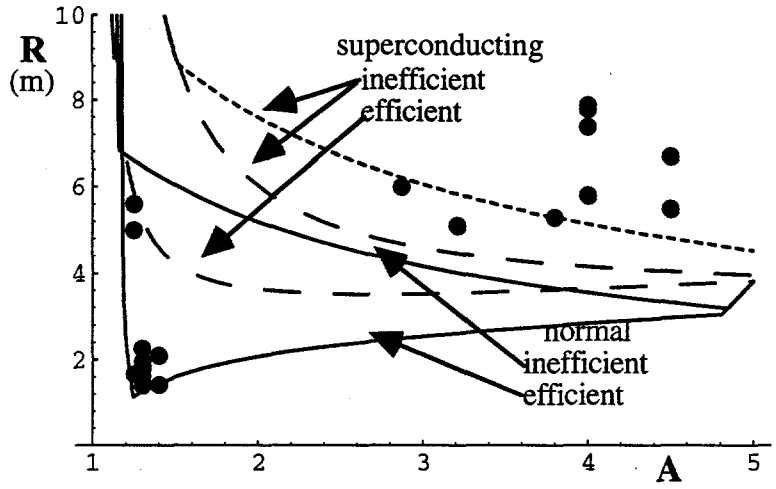

Figure 21. The device major radius for both superconducting (broken line) and normal copper (solid line) TF systems, for completely efficient (lower branch) and completely inefficient ($f_{bs} = 1$, upper branch) auxiliary current drive. The comparisons are made for $\beta_N = 3.5$, $\Gamma_n = 5\text{x}10^6$ Wm^{-2}, for both the $f_{bs} = 1$ (completely inefficient current drive, R independent of χ) and for completely efficient current drive with $\chi = 0.62$. Also shown as a dotted line is the superconducting, completely inefficient case with $\Gamma_n = 2\text{x}10^6$ Wm^{-2}. Other values are given in Table 3. The points correspond to the detailed studies presented in Table 1.

The usual operational mode is restricted by wall loading, or almost so, because of the strong dependence of the major radius on aspect ratio in the beta-limiting cases. It is shown in Part II (see also Appendix 2) that, for presently obtained values of auxiliary current drive efficiency, the major radius lies approximately half way between the two limits considered here in Part I. Then neither the superconducting nor the normal copper devices discussed above show any advantage in utilizing low A; V_m increases as A is decreased. The only counter example to this is if the scheme proposed utilizing reflected radiation to drive current is practical. Then it is permissible to invoke the limit of completely efficient current drive, and advantages in using low-A normal copper coils are possible. However, the reduction of a factor ≈ 2 in R_0 which follows for normal copper devices when A is reduced from ≈ 4 to ≈ 1.25 means that V_m is only reduced by $\approx 20\%$. That is, a lot of difficulties have been added for very little advantage.

Also shown in *Figure 21* are the data points for the designs described in Table 1. Note that the values of the variables necessary to deduce the analytic results (i.e. the values in Table 3) were chosen to represent typical values used in the detailed designs (i.e. the values in

Table 1). The low-A points, all for normal copper coils, are well described by the relevant simple model (solid lines). In particular the TARR designs [11,12] with the reflected radiation-driven plasma current correspond to the completely efficient current drive (allowing low q) while the LAR designs [3,6] correspond to the completely inefficient current drive ($f_{bs} = 1$, high q). The normal-A superconducting points all lie above the relevant analytic results (broken lines). The most relevant analytic case to consider for superconductors is the completely inefficient current drive limit, with $f_{bs} = 1$ (Section 3.5.2). The discrepancy is then at least partly reconciled by noting the strong dependence of the major radius with wall loading Γ_n (see Section 3.5.2.1 and *Figure 17*). The analytic curves described so far were derived for $\Gamma_n = 5\text{x}10^6\ \text{Wm}^{-2}$, while many of the detailed designs (see Table 1) use $\Gamma_n < 3\text{x}10^6\ \text{Wm}^{-2}$. That is, we have maintained Γ_n a constant for the comparisons between superconducting and normal copper coils, while the detailed designs do not do this. The dotted line in *Figure 21* shows the effect of decreasing Γ_n from $5\text{x}10^6\ \text{Wm}^{-2}$ to $2\text{x}10^6\ \text{Wm}^{-2}$ for the superconducting, $f_{bs} = 1$ case (completely inefficient current drive). The device major radius increases, and now there is better agreement between the analytic model and the detailed studies.

In the limit of $f_{bs} = 1$ the size of both the superconducting and normal copper devices is independent of the recirculating power fraction. This allows the power to the grid to be controlled, independent of machine major radius. This in turn allows a comparison between machines of different aspect ratio, but producing the same power to the grid, up to a value restricted by the product of the wall loading, the surface area and the conversion efficiency f_{el}. (Note that up to now we have not worried about the power to the grid in comparisons between devices). Therefore, for the cases considered, there is no advantage in utilizing low A either for devices in which any power to the grid is acceptable, or for devices in which a specified power is required, as long as that power does not exceed the maximum permissible at a given A. *Figure 22* shows the power to the grid P_{gr} for $\chi = 0$ (i.e. the maximum possible) as a function of A for wall loading limited ($\Gamma_n = 5\text{x}10^6\ \text{Wm}^{-2}$) superconducting TF and normal copper TF devices. Then for example devices with $P_{gr} =$ 0.5 MW can be designed with normal copper TF as long as $A < 2$, and from *Figure 21* we see that the optimum device (smallest V_m) in the range $A < 2$ is at $A = 2$.

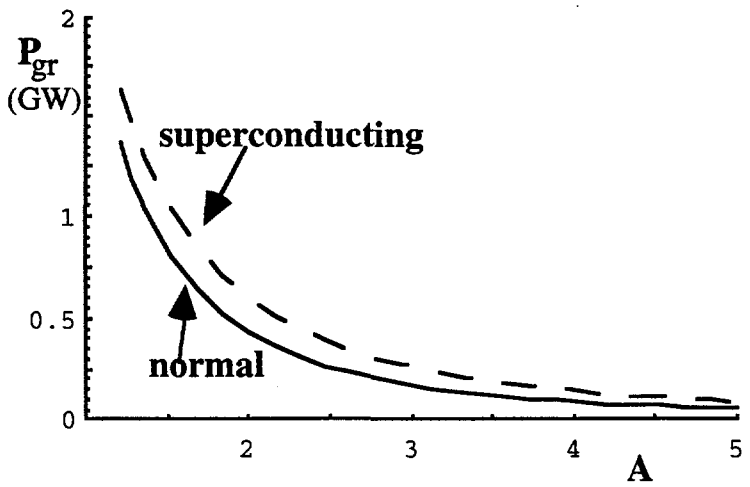

Figure 22. The maximum possible electric power to the grid P_{gr} for both normal copper TF (solid line) and superconducting TF (broken line), for fully bootstrap-driven devices, restricted by neutron wall loading to $\Gamma_n = 5\text{x}10^6\ \text{Wm}^{-2}$.

To advantage low-A, we next consider cases in which the normalized beta and elongation are allowed to increase with decreasing A. We choose $\beta_N = 9/\sqrt{A}$ and $\kappa = 3.5/\sqrt{A}$. The results for the $f_{bs} = 1$ case are shown in *Figure 23*, and there is remarkably little difference between the superconducting device and the normal copper device over most of the A-range shown. Also, although there is a slight decease in R with decreasing A, it is not enough to produce a V_m which decreases with decreasing A.

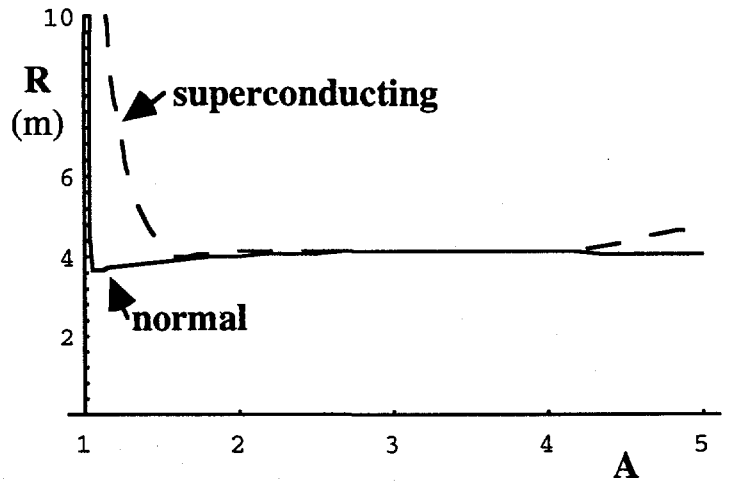

Figure 23. The major radius of devices with superconducting (broken line) and normal copper (solid line) TF systems, and 100% bootstrap current, with $\beta_N = 9/\sqrt{A}$, $\kappa = 3.5/\sqrt{A}$, $\Gamma_n = 5\text{x}10^6\ \text{Wm}^{-2}$, and other parameters as given in Table 3.

To demonstrate further that allowing large variations in κ and δ at low A can decrease R_0, but not V_m, we show *Figure 24a* and *Figure 24b*. Here are plotted contours of V_m as a

function of κ and δ for $A = 3.5$ (*Figure 24a*) and $A = 1.25$ (*Figure 24b*), in both cases for normal copper TF coils, major radii limited by wall loading to $\Gamma_n = 5\text{x}10^6\ \text{Wm}^{-2}$. In both cases we observe that at fixed A increasing either κ or δ reduces V_m, although the gains achieved by increasing δ at $A = 3.5$ are small. There may be other advantages of increasing δ such as increasing the β_N limit, but a sufficiently high β_N has already been achieved experimental: the wall loading is limiting. Referring to *Figure 24a)*, with a normal aspect ratio $A = 3.5$ we can expect to operate with $\kappa < 1.8$ to avoid axisymmetric instabilities, so that $V_m < 500\ \text{m}^3$. Referring to Figure 24b), we find that at low A it is not possible to achieve $V_m < 10^3\ \text{m}^{-3}$, even with $\kappa = 3.5$ and $\delta = 1$. Again we find that there is no advantage in operating at low A in the limits considered here

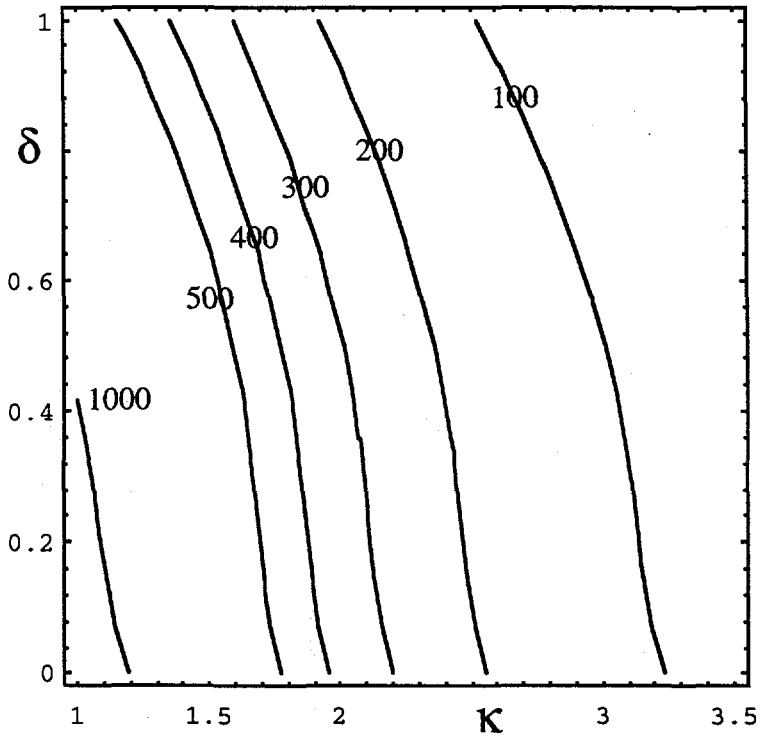

Figure 24a). Contours of V_m as a function of elongation κ and triangularity δ, for a wall loading limited copper TF coil system with $f_{bs} = 1$; aspect ratio $A = 3.5$.

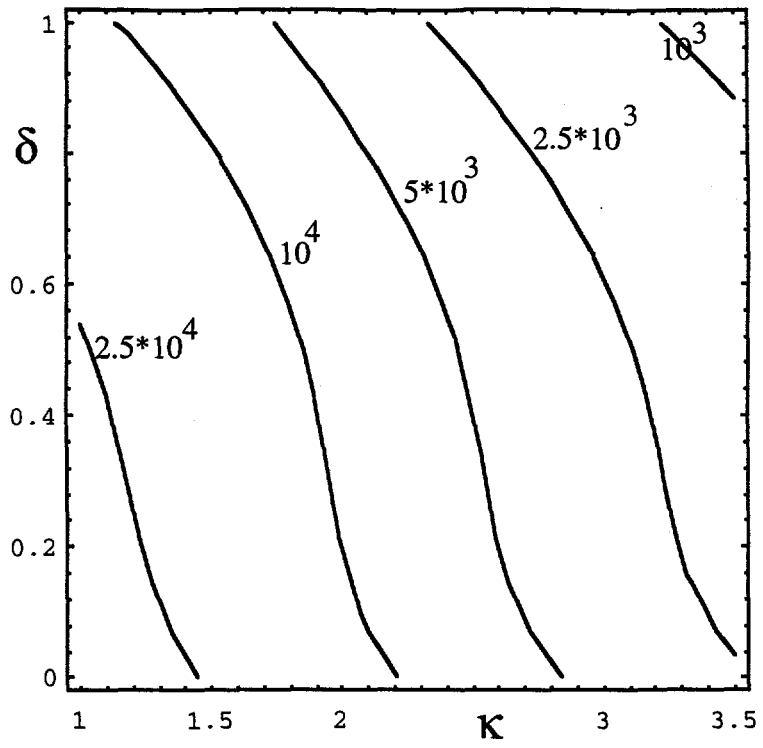

Figure 24b). Contours of V_m as a function of elongation κ and triangularity δ, for a wall loading limited copper TF coil system with $f_{bs} = 1$; aspect ratio $A = 1.25$.

Finally we discuss the effects of increasing the H factor for the case of a normal copper TF system with $f_{bs} = 1$. H can be increased until the β_N and Γ_n limited radii are equal. We consider the case which advantages low-A, namely $\beta_N = 9/\sqrt{A}$, $\kappa = 3.5/\sqrt{A}$, $\Gamma_n = 5\text{x}10^6$ Wm^{-2}, and other parameters as found in Table 3. Equating the two radii we find that for $A \approx 1.5$ then $H < 5$, otherwise the β_N limit is exceeded. There is only disadvantage in increasing H further at low A. This is illustrated in *Figure 25*, in which V_m is shown as a function of A for different H factors, for cases with $\beta_N = 9/\sqrt{A}$, $\kappa = 3.5/\sqrt{A}$, $\Gamma_n = 5\text{x}10^6$ Wm^{-2}, $\delta = 1$, and other parameters as found in Table 3. As H is increased the high-A β_N limit moves to lower A, and ultimately completely determines the device volume. For the conditions chosen there is a value of $H = 5.5$ where $A \approx 1.6$ is optimum, but a smaller volume V_m could have been chosen at lower H and higher A (e.g. $H = 4$, $A = 2.5$).

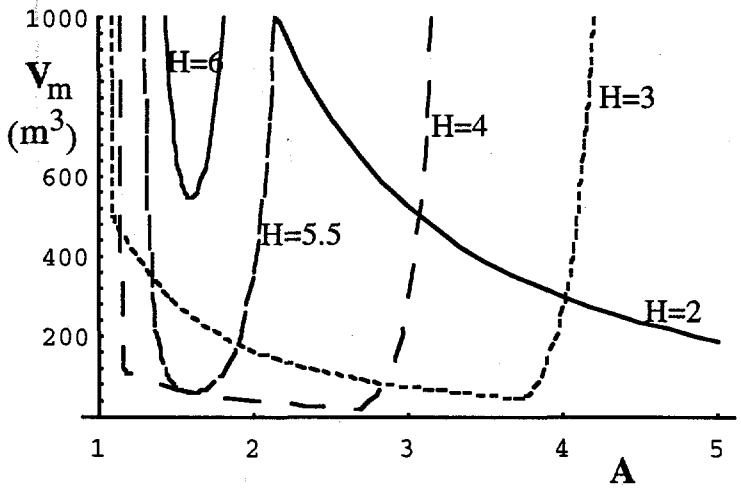

Figure 25. The machine encompassing volume V_m as a function of aspect ratio A for a normal copper TF coil system, $f_{bs} = 1$, with $\beta_N = 9/\sqrt{A}$, $\kappa = 3.5/\sqrt{A}$, $\delta = 1$, $\Gamma_n = 5 \times 10^6$ Wm^{-2}, and other parameters as found in Table 3. Results are shown for different H factors.

4. Scaling from a Given Design to a Low-*A* Copper Coil Design

Here we demonstrate that, given any reference reactor design, it is possible to assess whether a smaller copper coil device can be built at low aspect ratio. Consider a reference reactor (subscript 1) of known power to the grid P_{grl}, known geometry (A_1, R_1, a_1, κ_1, δ_1), known wall loading (Γ_1) and known profile factors and dilution (γ_{n1}, γ_{T1}, g_1). We will determine if a device with a smaller machine encompassing volume V_m can be built, with the same power to the grid and the same or smaller wall loading, at low A. We proceed as follows:

Known geometry of reference reactor $\Rightarrow V_{m1}$ known
Let machine encompassing volume of test device be $V_{m2} = \varphi V_{m1}$.
Choose aspect ratio A_2 , elongation κ_2 and triangularity δ_2 of test (low-A) device.
$\Rightarrow$ major radius $R_2(\varphi, A_2, \kappa_2, \delta_2)$ of the test device.
$\Rightarrow$ volume $V_{p2}(\varphi, A_2, \kappa_2, \delta_2)$ and surface area $S_2(\varphi, A_2, \kappa_2, \delta_2)$
$\Rightarrow$ (with $\Gamma_2 = \Gamma_1$) fusion powers $P_{n2}(\varphi, A_2, \kappa_2, \delta_2)$ and $P_{\alpha 2}(\varphi, A_2, \kappa_2, \delta_2)$

$P_{n2}(\varphi, A_2, \kappa_2, \delta_2) \Rightarrow$ (with P_{grl} and $f_{el2}(A_2, \kappa_2, \delta_2)$ the electric power
$P_{el2}(A_2, \kappa_2, \delta_2)$ and the recirculating power fraction $\chi_2(\varphi, A_2, \kappa_2, \delta_2)$,
$\Rightarrow$ (with f_{TF2}) the TF power $P_{TF2}(\varphi, A_2, \kappa_2, \delta_2)$
$\Rightarrow B_{T02}(\varphi, A_2, \kappa_2, \delta_2)$ and $B_{Tleg2}(\varphi, A_2, \kappa_2, \delta_2)$

$P_{\alpha 2}(\varphi, A_2, \kappa_2, \delta_2) \Rightarrow$ (with V_{p2}, dilution, profiles) pressure $p_2(\varphi, A_2, \kappa_2, \delta_2)$ and
energy $W_2(\varphi, A_2, \kappa_2, \delta_2)$
$\Rightarrow$ (with B_{T02}) $\beta_{T2}(\varphi, A_2, \kappa_2, \delta_2)$, $\tau_{E2}(\varphi, A_2, \kappa_2, \delta_2) = W_2/P_{\alpha 2}$
a) completely inefficient current drive (100% bootstrap):
$\Rightarrow$ safety factor $q_2(\varphi, A_2, \kappa_2, \delta_2)$
b) completely efficient current drive:
$\Rightarrow$ safety factor $q_2 = 3.2$
$\Rightarrow$ (with geometry) $I_{p2}(\varphi, A_2, \kappa_2, \delta_2)$
$\Rightarrow$ (with B_{T02}, geometry, maximum $T_{0,max}$) the maximum β (either Troyon limit, or Greenwald limit)

That is, the properties of the test device (subscript 2) are now completely specified as functions of φ, A_2, κ_2, and δ_2. The test device with the smallest encompassing volume at

a given A is found by reducing φ, allowing κ_2 and δ_2 to vary over specified limits, until β reaches the maximum allowed, either the Troyon limit or the Greenwald limit.

Figure 26 shows an example, in which the test reactor has $V_{rl} = 909$ m^3, $\Gamma_l = 5$ MWm^{-2}, and $P_{grl} = 962$ MW, values typical of superconducting reactor scenarios. Plotted is the minimum possible φ and the associated H factor (with respect to the Goldston scaling value) against aspect ratio A. The allowed variations in geometry are $0 < \delta < 1$ and $1 < \kappa < 3.5/\sqrt{A}$, with $\beta_N = 9/\sqrt{A}$. This assumed dependence of the maximum permissible κ on A gives great advantage to low-A. For the example with completely inefficient current drive, or 100% bootstrap current, then *Figure 26a* shows $\phi > 1$ for all A, and the smallest low-A device is larger than the normal-A device. Even if completely efficient current drive is possible, then *Figure 26b* shows that $\phi > 1$. In all cases the H factor is reasonable, and drops below 1 for the completely efficient case (*Figure 26b*)

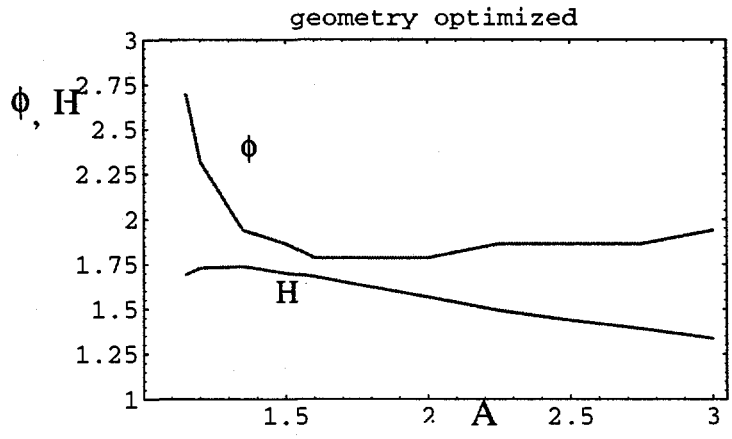

Figure 26a. The minimum φ and H factor as a function of A of a test reactor, 100% bootstrap current (completely inefficient current drive) for a reference case in which $V_{rl} = 909$ m^3, $\Gamma_l = 5$ MWm^{-2}, and $P_{grl} = 962$. The optimization is performed for $0 < \delta < 1$ and $1 < \kappa < 3.5/\sqrt{A}$, with $\beta_N = 9/\sqrt{A}$.

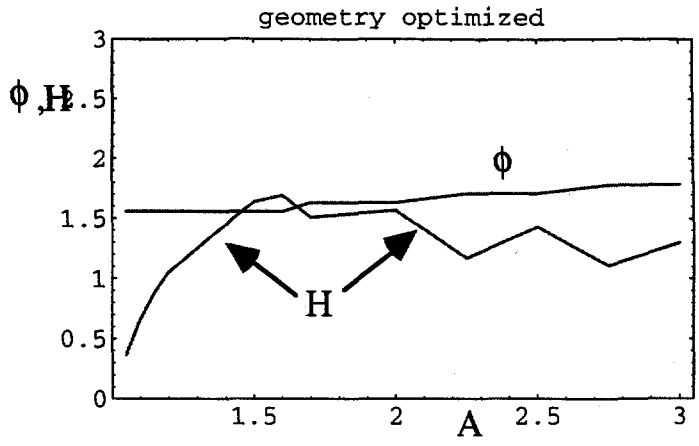

Figure 26b. The minimum φ and H factor as a function of A of a test reactor, $q = 3.2$ (completely efficient current drive) for a reference case in which $V_{ml} = 909$ m^3, $\Gamma_l = 5$ MWm^{-2}, and $P_{grl} = 962$. The optimization is performed for $0 < \delta < 1$ and $1 < \kappa < 3.5/\sqrt{A}$, with $\beta_N = 9/\sqrt{A}$.

5. Summary and Conclusions

First, a survey of various tokamak reactor designs shows that they fall into three regions of (R,A) space. The superconducting devices are clustered around ($R \approx 6$ m, $A \approx 4$). The low-A normal copper devices, or ST's, are found either around ($R \approx 5$ m, $A \approx 1.3$), or around ($R \approx 2$, $A \approx 1.3$). In order to understand these groupings, an analytic model for the size of the smallest tokamak reactor has been presented. This model is not intended to supplant detailed studies, but rather to provide an understanding of various limits and scalings. Using a steady state energy balance, together with a simple scaling relationship for the energy confinement time, the machine architecture is found as a function of, in particular, safety factor q and toroidal field B_T. These in turn can be specified for two limits of auxiliary current drive efficiency, either completely inefficient (so that reliance must be placed on bootstrap current, which restricts q) or completely efficient, so that q can be chosen at will. Results relevant both to copper toroidal field coils, with the attendant ohmic losses in the toroidal field coils, and superconducting coils, are presented. The copper coil model is expected to be more accurate than the superconducting coil model; the dominant ohmic losses in the copper toroidal field coil are well represented, whereas many losses in the superconducting system are ignored.

Three restrictions are imposed, due to wall loading, normalized beta and absolute beta limits. In addition it is verified that the density and temperature are consistent with the Greenwald limit and the fit to the reaction cross sections. Table 4 then summarizes where the relevant equations describing the size of the twelve machines can be found, given the coil type (normal copper or superconducting), the current drive efficiency limit (completely efficient or completely inefficient), and the relevant restriction. Appendix 2 shows that using a presently achieved auxiliary current drive efficiency of $\eta_{CD} = 1\text{x}10^{19}$ $\text{AW}^{-1}\text{m}^{-2}$ leads to results closer to the analytic completely inefficient limit than to the analytic completely efficient limit; more details of arbitrary current drive efficiency, and other scaling relations, will be presented in Part II.

The analytic results are used for three purpose; a discussion of the published reactor design geometry, a comparison between normal copper and superconducting coil reactors, and optimization of low-A copper toroidal field coil devices. First, comparing the detailed point designs with the analytic model show that the three groupings in (R,A) space are readily understood (see *Figure 21*). The low-A points, all for normal copper coils, are well

described by the relevant simple model. In particular the TARR designs [11,12] with the reflected radiation-driven plasma current correspond to the completely efficient current drive (allowing low q) while the LAR designs [3,6] correspond to the completely inefficient current drive ($f_{bs} = 1$, high q). The normal-A superconducting points are also approximately described if allowance is made for the differing neutron wall loading values assumed.

Second, the possible advantages of low-A copper coil devices over superconducting coil devices are discussed. The published detailed studies show a reduction in R of approximately a factor three can be achieved if very efficient auxiliary current drive is invoked at low A , but is not invoked for the normal-A superconducting case. Part of the reduction is because the low-A copper devices often utilize a larger neutron wall loading than the superconducting devices; without this a reduction in R of approximately a factor two is possible. However, if it is considered that it is not R which is important, but rather the machine encompassing volume V_m, then any reductions in V_m, even with very efficient current drive, are minimal.

Third, optimization of device size using the analytic model results is presented. Although formulae and scalings relevant to superconducting devices are given, the emphasis here is on low-A normal copper toroidal field coil systems. In most cases the neutron wall loading Γ_n is the restricting parameter, with existing β_N limits being sufficiently large that their effects, namely restricting very low A and high A, are not significant. For completely efficient current drive $R_\Gamma \propto \left[q^2 / \chi \Gamma_n H^2\right]^{0.36}$. That is, increasing the allowed recirculating power fraction χ, wall loading Γ_n, or confinement factor H, or decreasing the allowed safety factor q, allows a smaller machine to be built. For completely inefficient current drive $R_{\Gamma bs} \propto H^{-1.6}\Gamma_n^{-0.4}\chi^0$. The major radius of the smallest device with $f_{bs} = 1$ is thus independent of the recirculating power fraction χ, but increasing χ increases the field at the toroidal field leg $B_{Tleg,\Gamma bs}$ and the safety factor $q_{\Gamma bs}$. This lack of a dependence of $R_{\Gamma bs}$ on χ means that the power to the grid, $P_{gr} = f_{el}P_n(1-\chi) = f_{el}S\Gamma_n(1-\chi)$, is controlled by changing χ, i.e. by changing $B_{Tleg,\Gamma bs}$. Increasing confinement (increasing H) decreases $R_{\Gamma bs}$, $B_{Tleg,\Gamma bs}$ and $q_{\Gamma bs}$. Increasing the permitted neutron wall loading Γ_n decreases $R_{\Gamma bs}$, but increases $B_{Tleg,\Gamma bs}$. H can only be increased until the β_N and Γ_n limited radii are equal; further increases in H increase R.

We observe that at fixed A increasing either elongation κ or triangularity δ reduces V_m, although the gains achieved by increasing δ at A = 3.5 are small. In an attempt to advantage low-A, the normalized beta and elongation were allowed to increase with

decreasing A . We chose $\beta_N = 9/\sqrt{A}$ and $\kappa = 3.5/\sqrt{A}$. For the completely inefficient current drive case the results (*Figure 23*) showed little difference between the superconducting device and the normal copper device over most of the A-range considered. Also, although there was a slight decease in R with decreasing A, it is not enough to produce a V_m which decreases with decreasing A. Only for the completely efficient current drive case (*Figure 27*) were advantages in obtaining reduced V_m at low-A. For these very optimistic conditions there is a value of $H = 5.5$ where $A \approx 1.6$ is optimum, but a smaller volume V_m could have been chosen at lower H and higher A (e.g. $H = 4$, $A = 2.5$).

The final conclusion is that, if low-A devices are to be used as power plants, then the only advantageous route to low machine encompassing volume presently envisaged, as demonstrated both by the published designs and the simple models descried here, is to invoke large elongation, large wall loading, and very efficient (approaching completely efficient) current drive schemes.

6. References

[1] Y-K. M. Peng, Transactions of Fusion Technology 27 138 (1995).

[2] *Fusion Materials, Semiannual Progress Report for the Period Ending March 31*, 1994, Report DOE/ER-0313/16, pages 313-368, The U.S. Department of Energy (1994).

[3] C. G. Bathke and the ARIES Team, "A Preliminary Systems Assessment of the Starlite Demo Candidates", Proc. 16th IEEE/NPSS Symp. on Fusion Engineering, Champaign, IL., Oct. 2-5, 1995, Los Alamos Report LA-UR-95-3489, Rev. 10/12/95 (1995).
(Note that all these designs are costed in 1992 dollars. The SS case has been re analyzed on the same physics basis as the RS and the CoE increased. The appropriate conclusion is that RS is better than SS. (C. G. Bathke, private communication)).

[4] C. G. Bathke, R. L. Miller, and the Aries Team, "Evolution of the Aries-I Design in the ARIES and PULSAR Projects", Proc. 16th IEEE/NPSS Symp. on Fusion Engineering, Champaign, IL., Oct. 2-5, 1995, Los Alamos Report LA-UR-95-3429, Rev. 10/12/95 (1995).

[5] J. D. Galambos, L. J. Perkins, S. W. Haney and J. Mandrekas, Nucl. Fus. 35 (5), 551 (1995).

[6] F. Najmabadi (Ed.) "The Starlite Project -- The Assessment Phase Report", to be published as a UCSD Report.
(LSA = 2. LAR-2 is an optimized version of LAR-1, with 100% bootstrap)

[7] V. Chan, "Fusion Development Paths", presented at the Starlite Town Meeting on low Aspect Ratio Tokamaks, UCSD, Jan. 31, 1996.

[8] R. A. Krakowski," Low-Aspect-Ratio Fusion Power Plants", ORNL Workshop on Establishing the Physics Basis Needed to Asses the Potential of Compact Toroidal Reactors, July 19-22, 1994.
(LSA = 3, CoE in 1986 $)

[9] T. C. Hender, D. C. Robinson, P. J. Knight and H. Wilson, "Self Consistent Tight Aspect Ratio Reactors," private communication (1995).

[10] Y. M. Peng and J. Sheffield, "The Spherical Tokamak Reactor", Spherical Tokamak Workshop and U.S.-R. F. GLOBUS Exchange, Oct. 12-16, Oak Ridge, TN (1992).

[11] R. Hancox, "TART Reactor Studies", Spherical Tokamak Workshop, ORNL, Oct., 1992.

[12] T. C. Hender, L. J. Baker, R. Hancox, J. B. Hicks, P. J. Knight, D. C. Robinson and H. R. Wilson, "Tight Aspect Ratio Tokamak Reactors", in Plasma Physics and Controlled Nuclear Fusion Research 1992, 14 th Conference Proceedings, Wurtzburg, Germany, 30 September - 7 October 1992, 3 399 (1992) (Rebut-Lallia scaling).

[13] R. J. Goldston, Plasma Phys. Controlled Fusion 26 87 (1984).

[14] S. M. Kaye, C. W. Barnes, M. G. Bell *et al.*, Phys. Fluids B2 2926 (1990).

[15] A. Sykes, Plasma Phys. Control. Fusion 36 B93-B106 (1994).

[16] M. Gryaznevich, R. J. Colchin, R. Duck *et al.*, in Proceedings of the 21 st European Phys. Soc. Conference on Controlled Fusion and Plasma Physics, Montpellier, (European Physical Society, 1994), Vol. 18B, Part 1, 22 (1994).

[17] J. M. Dawson and P. K. Kaw, Phys. Rev. Letts. 48 1730 (1982).

[18] D. W. Ross, "Definition of total bootstrap current in tokamaks", Fusion Research Center Report FRCR #473, DOE/ER/54296-52 (1995).

[19] F. Troyon, R. Gruber, H. Saurenmann *et al.*, Plasma Phys. Controlled Fusion 26 209 (1984).

[20] M. Greenwald, J. L. Terry, S. M. Wolfe et al., Nucl. Fusion 28 2199 (1988).

[21] N. A. Uckan, Fus. Tech. 15 391 (1989).

[22] P.-H. Rebut, P. P. Lallia and M. L. Watkins, in Plasma Physics and Controlled Nuclear Fusion Research 1988 (Proc. 12 th Int. Conf. Nice, 1988), Vol. 2, IAEA Vienna (1989) 191.

[23] J. P. Holdren *et al.*, "Report of the Senior Committee on Environmental , Safety, and Economic Prospects of Fusion Reactors", Lawrence Livermore National Laboratory report UCRL-53766 (1989).

[24] Y-K. M. Peng and D. J. Strickler, Nucl. Fusion 26 769 (1986).

[25] See reference 8 for a comparison of a low and a high aspect ratio design. The peak neutron flux (neutron wall loading) is approximately 30% higher than the average, and occurs at the outer equator.

[26] H. Wilson, Nucl. Fusion 32 257 (1992)

[27] S. P. Hirshman, Phys. Fluids 31 3150 (1988).

[28] W. M. Nevins, presented at the U.S.-Japan Workshop on Bootstrap Current, Lake Lanier Islands, GA, Nov. 2-4, 1994.

[29] NSTX Proposal, 1995, Fig. 2.4

[30] S. Kaye, presented at the FEAC Scicom Meeting, Austin, Feb. 27, 1996.

[31] G. C. Bathke, Systems Assessment of Low-Aspect Ratio Power-Plants, private communication (1995)

7. Appendices

7.1. Surface Areas and Volumes

The plasma surface is described by the Equation $R = R_0 + x$ with $x = a\cos(\alpha + \delta\sin\alpha)$ and $y = a\kappa\sin\alpha$, where δ is the triangularity and κ the vertical elongation of the cross section. This geometric description is a good fit to the analytic equilibria found in [??].

Surface area. This is approximated by the fit

$$S = 2\pi^2 Ra(1+\kappa)\left(1 - \frac{0.13\delta\kappa^{0.25}}{A}\right)$$

The δ dependence is weak.

Ratio of outer to total surface area. This ratio is used to calculate the fraction of neutrons available for electricity generation (assuming a uniform wall loading). It is approximated by the fit

$$\frac{S_{outer}}{S_{total}} = \left(\frac{1}{2} + \frac{\kappa^{0.13}}{\pi A}\right)\left(1 + 0.3\delta\kappa^{-0.5}\right)$$

which is exact for a circle, and accurate to better than 5% for $\delta = 0$. The dependence on δ is very weak.

Volume. Performing an expansion in δ, we find

$$V = 2\pi^2 R\kappa a^2\left(1 - \frac{\delta}{4A} - \frac{\delta^2}{8}\right)$$

Again, for the aspect values of interest, the δ dependence is very weak.

TF coil inner leg resistance. This is defined by the integral

$$\int \frac{dy}{(R - a'(y) - w_b)^2}$$

where w_b is the inner blanket thickness, and a' is the horizontal distance between the plasma center (at R_0) and the plasma surface, a function of the vertical height y. The

integration is from the lowest to highest points in the plasma, and the resulting power consumed is well approximated by the expression

$$P_{TF} = \frac{8\eta\pi\kappa B_{T\max}^2 R_0}{\mu_0^2 f_{Cu} A}\left(1 - e^{-1.3\omega\sqrt{A - A_{\min}}}\right)$$

where

$$\omega = \left(1 + \frac{2}{3}\delta\right) / \left(1 - \frac{2}{3}\delta\right)$$

and

$$A_{\min} = \frac{1}{1 - w_b}$$

The dependence on δ is important, and retained in all calculations. For $\delta = 1$ the expression reverts to that for a straight cylindrical column, the most resistive case.

7.2. Arbitrary Current Drive Efficiency

In this work (Part I) we have dealt with one particular scaling relationship, and two extremes of current drive efficiency, and found we can understand the geometry of the published reactor studies. An important consequence is that only if completely efficient current drive is invoked can gains in reducing the machine encompassing volume be achieved by using low-A and copper toroidal field coils. Even in this extreme the reductions in V_m are small, e.g. 20%.

Part II of this work will detail numerical calculations of the smallest copper coil device with arbitrary current drive efficiency and with many different scaling relationships. Here we show only one of the numerical results, namely that the analytic limits are validated by the numerical calculations, and that a realizable current drive efficiency ($\eta_{CD} \approx 1\text{x}10^{19}$ AW^{-1}m^{-2} [2 to 12]) produces a device with a major radius approximately half way between the values predicted by the 'completely inefficient' $f_{bs} = 1$ case and the 'completely efficient' case considered in Part 1.

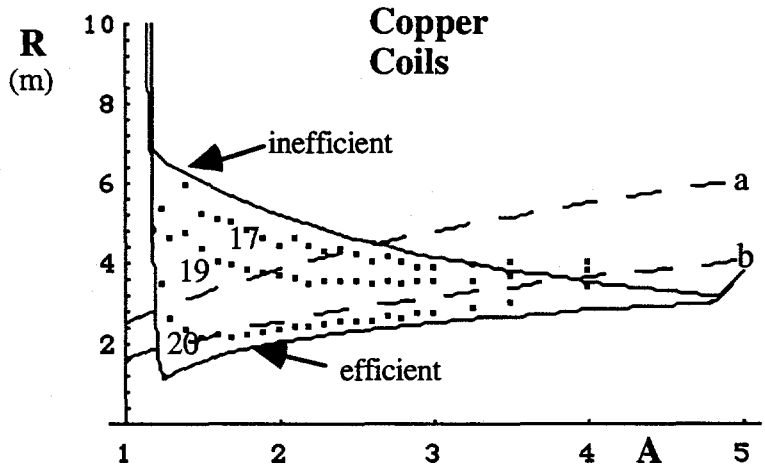

Figure 27. The major radius R of the smallest copper coil device as a function of aspect ratio A. Solid lines: analytic model, both completely efficient and completely inefficient limits. Points: values obtained from the numerical calculation for three different current drive efficiencies, $\eta_{CD} \approx 1\text{x}10^{17}$ AW^{-1}m^{-2} (marked as 17), $\eta_{CD} \approx 1\text{x}10^{19}$ AW^{-1}m^{-2} (marked as 19), and $\eta_{CD} \approx 1\text{x}10^{20}$ AW^{-1}m^{-2} (marked as 20). The broken lines are curves of constant machine encompassing volume V_m (constant κ). Other parameters are as described for *Figure 21*, and found in Table 3.

Figure 27 shows a comparison between the analytic and the numerical results. The analytic results (solid lines) were obtained with the parameters used to construct *Figure 21*, that is

$H = 2$, $\Gamma_n = 5$ MWm^{-2}, $\chi = 0.62$, $\beta_N = 3.5$ and $\kappa = 2$, with other values found in Table 3. The numerical results allowed Γ_n, χ, β_N and κ to vary up to the values used in the analytic work. In addition, the numerical model allowed P_{CD} to vary, and the smallest device was then found at any given A. Three different current drive efficiencies were used in the numerical modeling; a very efficient $\eta_{CD} = 10^{20}$ AW^{-1}m^{-2}, an intermediate $\eta_{CD} = 10^{19}$ AW^{-1}m^{-2}, and an inefficient $\eta_{CD} = 10^{17}$ AW^{-1}m^{-2}. The analytic limits and the numerical results with the extreme values of η_{CD} are in reasonable agreement; the numerical results obtained using the typical value of η_{CD} lie between the two analytic limits. Also shown in the figure, as a broken lines, are curves of constant machine encompassing volume V_m for constant κ. That is, they represent $R \propto A/(A-1)^{2/3}$. The upper curve, labeled a, is drawn through a point with $R = 5.5$ m, $A = 4$, that is, a point representative of the superconducting coil designs available in the literature (see Table 1). The lower curve, labeled b, is drawn through a point with $R = 2$ m, $A = 1.3$, that is, a point representative of the lowest R normal copper coil designs (see Table 1).

Any designs with a major radius R below curve a then have a smaller machine encompassing volume V_m that the superconducting machines considered in the literature (although note that the designs in the literature advantage low-A by using a higher neutron wall loading at low-A). Therefore advantages are found at the lowest $A \approx 1.3$ only if very efficient current drive schemes are invoked (with $\eta_{CD} > 10^{20}$ AW^{-1}m^{-2}). Any designs with R below curve b are designs with a smaller V_m than the most optimistic normal copper coil ST's considered in the literature. Then with $A \approx 4$ there is than a normal copper coil design with V_m smaller than that of the lowest A cases. Whereas the lowest A, lowest R cases in the literature invoke remarkably efficient current drive, the copper coil case with $A \approx 4$ would require only an inefficient current drive system, relying instead on a high bootstrap fraction. That is, the optimum device is a high field, normal copper coil machine relying on a high bootstrap fraction.